# Extracellular vesicles are carriers of adiponectin with insulin-sensitizing and anti-inflammatory properties

Alexia Blandin, Jérémy Amosse, Josy Froger, Gregory Hilairet, Maëva Durcin, Lionel Fizanne, Valentine Ghesquière, Xavier Prieur, Julien Chaigneau, Luisa Vergori, et al.

Cell Reports

Article

# Extracellular vesicles are carriers of adiponectin with insulin-sensitizing and anti-inflammatory properties

## Graphical abstract

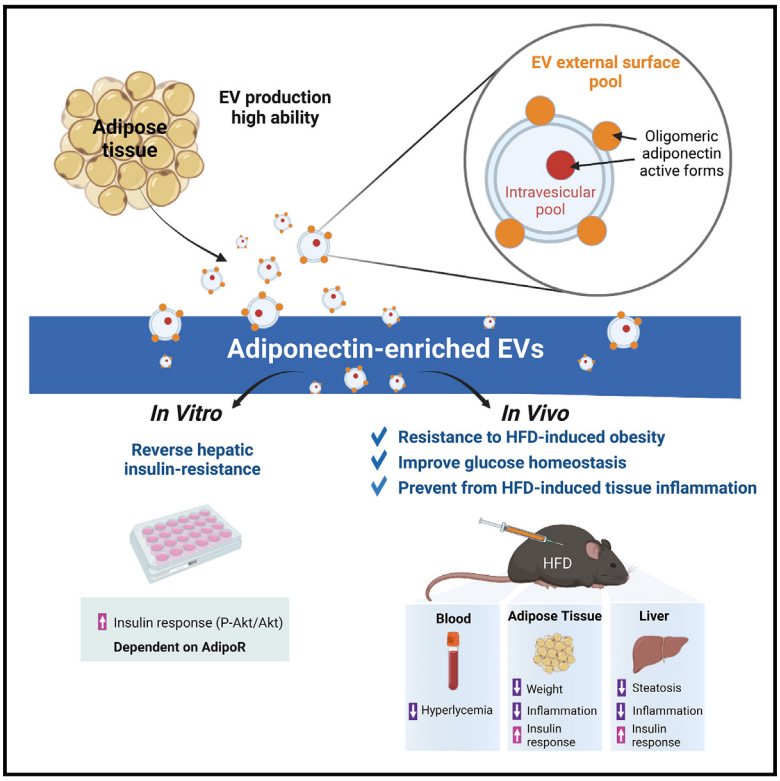


## Highlights

- Adiponectin is abundantly associated with adipose-tissue-derived sEVs
- sEVs constitute stable conveyors of adiponectin in the blood circulation
- Adiponectin-enriched sEVs display insulin-sensitizing effects *in vitro* and *in vivo*
- Adiponectin-enriched sEV injections in mice reduce HFD-induced tissue inflammation


## Authors

Alexia Blandin, Jérémy Amosse, Josy Froger, ..., Jérôme Boursier, Bertrand Cariou, Soazig Le Lay

## Correspondence

soazig.lelay@inserm.fr



## In brief

Blandin et al. show that adipose-tissue-derived sEVs act as stable conveyors of adiponectin in the blood that relay insulin-sensitizing action of the adipokine. Adoptive transfer of adiponectin-enriched sEVs in mice prevents animals from high-fat-diet weight gain, insulin resistance, and tissue inflammation, highlighting sEVs as delivery platforms of adiponectin active forms.


Blandin et al., 2023, Cell Reports *42*, 112866
August 29, 2023 
https://doi.org/10.1016/j.celrep.2023.112866

CellPress

Cell Reports

CellPress
OPEN ACCESS

Article

# Extracellular vesicles are carriers of adiponectin with insulin-sensitizing and anti-inflammatory properties

Alexia Blandin,[1,2,10,11] Jérémy Amosse,[2,3,11] Josy Froger,[1,2,11] Grégory Hilairet,[2] Maëva Durcin,[2] Lionel Fizanne,[4] Valentine Ghesquière,[1,2] Xavier Prieur,[1] Julien Chaigneau,[4] Luisa Vergori,[2] Cédric Dray,[5] Jean-Philippe Pradère,[5] Stéphanie Blandin,[6] Joëlle Dupont,[7] Pierre-Henri Ducluzeau,[7,8] Séverine Dubois,[9] Jérôme Boursier,[4,9] Bertrand Cariou,[1] and Soazig Le Lay[1,2,12,*]

[1]L'Institut du Thorax, CNRS, INSERM, Nantes Université, 44000 Nantes, France
[2]Université Angers, *SFR* ICAT, 49000 Angers, France
[3]IRSET Laboratory, Inserm, UMR 1085, Rennes, France
[4]HIFIH, CHU Angers, Université Angers, *SFR* ICAT, 49000 Angers, France
[5]RESTORE, UMR 1301 Inserm, 5070 CNRS, Université Paul Sabatier, Toulouse, France
[6]CHU Nantes, CNRS, Inserm BioCore US16, SFR Bonamy, Nantes Université, 44000 Nantes, France
[7]CNRS, IFCE, INRAE, PRC, Université de Tours, 37380 Nouzilly, France
[8]Service de Médecine Interne, Unité d'Endocrinologie Diabétologie et Nutrition, Centre Hospitalier Universitaire et Faculté de Médecine, Université de Tours, Tours, France
[9]CHU Angers, Angers, France
[10]L'institut du Thorax, CNRS, INSERM, CHU Nantes, Nantes Université, 44000 Nantes, France
[11]These authors contributed equally
[12]Lead contact
*Correspondence: soazig.lelay@inserm.fr
https://doi.org/10.1016/j.celrep.2023.112866

## SUMMARY

Recent evidence supporting that adipose tissue (AT)-derived extracellular vesicles (EVs) carry an important part of the AT secretome led us to characterize the EV-adipokine profile. In addition to evidencing a high AT-derived EV secretion ability that is further increased by obesity, we identify enrichment of oligomeric forms of adiponectin in small EVs (sEVs). This adipokine is mainly distributed at the EV external surface as a result of nonspecific adsorption of soluble adiponectin. EVs also constitute stable conveyors of adiponectin in the blood circulation. Adiponectin-enriched sEVs display *in vitro* insulin-sensitizing effects by binding to regular adiponectin receptors. Adoptive transfer of adiponectin-enriched sEVs in high-fat-diet-fed mice prevents animals from gaining weight and ameliorated insulin resistance and tissue inflammation, with major effects observed in the AT and liver. Our results therefore provide information regarding adiponectin-related metabolic responses by highlighting EVs as delivery platforms of metabolically active forms of adiponectin molecules.

## INTRODUCTION

More than 25 years ago, the discovery of leptin and adiponectin highlighted adipose tissue (AT) as a key player in the interorgan regulation of energetic metabolism through endocrine signaling.[1] Epidemiological studies concordantly supported that plasma adiponectin levels were inversely correlated with insulin resistance, arguing in favor of an insulin-sensitizing action of this adipokine.[2] Consistently, early experiments demonstrated that recombinant adiponectin improves insulin action in various mouse models of severe insulin resistance.[3] A large body of work has demonstrated that adiponectin exerts beneficial effects on several target tissues, including AT, liver, muscle, heart, kidney, and pancreas.[4] However, despite multiple studies showing that increasing adiponectin action has therapeutic potential for the treatment of type 2 diabetes (T2D), the complexity of the adiponectin structure strongly hampers the development of recombinant adiponectin as a therapeutic strategy for T2D.[5]

In addition to hormonal communication, extracellular vesicles (EVs) are mediators of cell-to-cell communication that participate in the development of various pathologies.[6] Adipocyte-derived EVs have recently emerged as important mediators of obesity-associated metabolic dysfunctions.[7] EVs are membrane-derived vesicle subtypes that differ in size, origin, and composition.[8] EVs encompass exosomes (with a diameter between 30 and 150 μm), formed as intraluminal vesicles of internal multivesicular compartments of the endocytic pathway (MVB) and plasma membrane-derived microvesicles/ectosomes of larger sizes (over 100 μm and up to 1 μm). Nonetheless, the absence of specific EV subtype markers renders it difficult to firmly establish the respective biogenesis pathway of small EVs (sEVs) or large EVs (lEVs).[9] All EVs are secreted in the

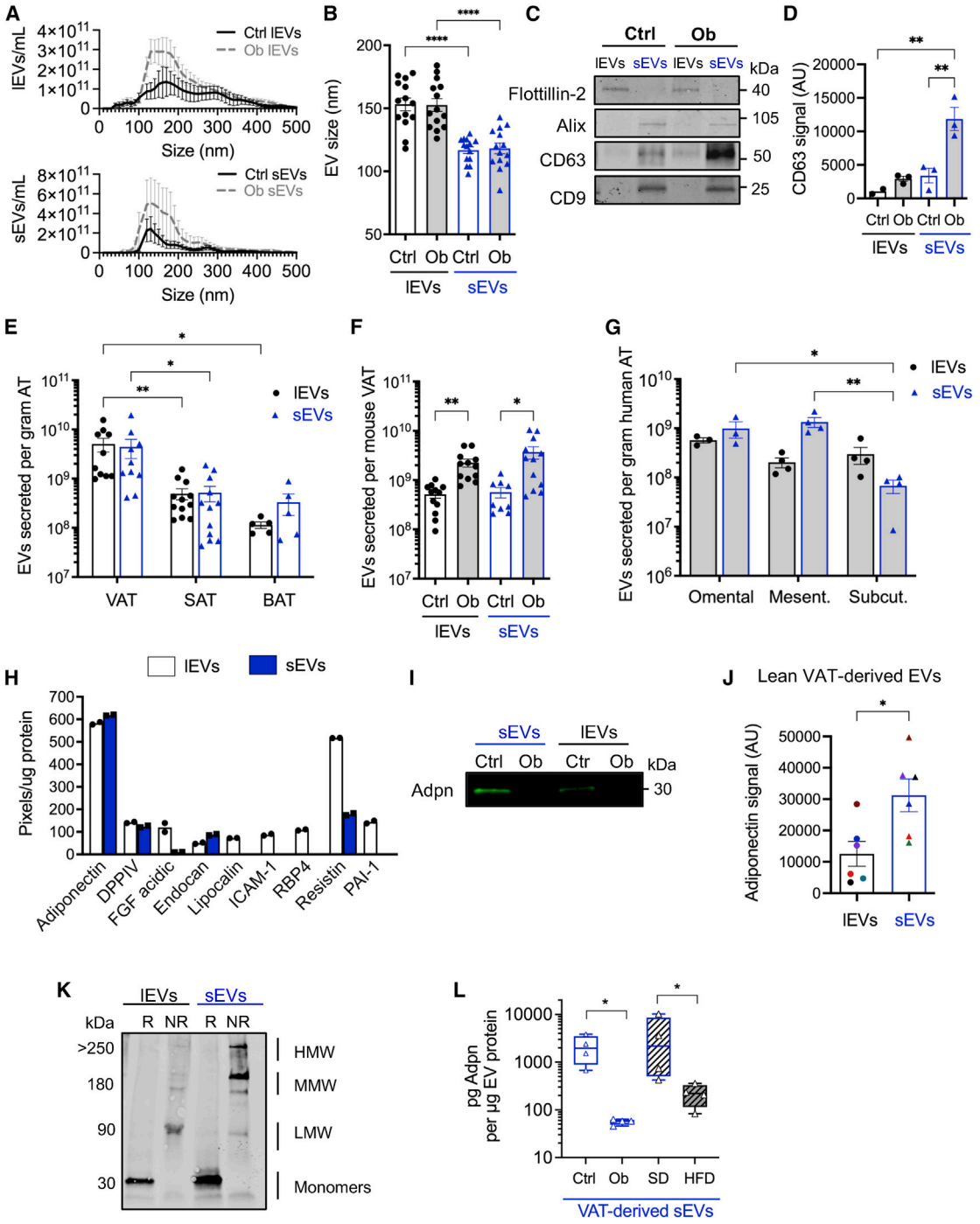


**Figure 1. Adiponectin is the most enriched adipokine in VAT-derived EVs**

(A and B) Lean (Ctrl) and obese (Ob) VAT-derived IEV and sEV mode size comparison. Size-distribution curves (A) and mean mode size (B). Ctrl and Ob EV subtype size-distribution curves (A) are represented by plain or dashed lines, respectively, and are presented as the mean ± SEM (n = 4–6 independent EV preparations for each condition).

(C and D) EV marker analysis from lean (Ctrl) or *ob/ob* (Ob) VAT explant-derived EV subpopulations. A significant enrichment in CD63 was observed for obese VAT-derived sEVs (D).

(E) IEV and sEV secretion from VAT, SAT, and BAT explants. EV number secreted per gram of AT per 24 h is presented.

(F) Increased IEV and sEV secretion from mouse VAT with obesity. EV secreted by total mouse VAT is presented.

(G) EV secretion of human omental, mesenteric (Mesent.), and subcutaneous (Subcut.) AT collected from obese subjects. Secretion of EVs is presented as the number of EVs secreted per gram of human AT.

*(legend continued on next page)*

extracellular space and circulate via biofluids, allowing EVs to exert paracrine or endocrine effects. Circulating EV levels were found to be increased in obese people in comparison with lean healthy subjects.[10–12] Moreover, EV plasma levels were correlated with body mass index (BMI) and homeostatic model assessment of insulin resistance, suggesting a potential role of EVs in the pathogenesis of T2D.[11–14]

We previously documented the ability of adipocytes to secrete high quantities of lEVs and sEVs, which display specific protein and lipid signatures.[15] Adipocyte-derived EV secretion is induced by lipid and inflammatory signals, two metabolic traits of obesity.[15–17] Accordingly, sEV secretion by AT is enhanced in different preclinical models of obesity.[18,19] Blood injections of obese AT-derived sEVs into lean mice promoted whole-body insulin resistance when compared to injections of lean AT-derived sEVs.[18] The metabolic effects of adipocyte-derived sEVs rely on the intercellular transfer of EV cargoes, including genetic material, proteins, lipids, or even organelles. AT-derived sEVs serve as carriers of microRNA (miRNA),[20,21] adipokines,[22] proteins,[23] neutral lipid carriers,[24] or mitochondria,[25] illustrating a versatile and complex mode of communication that participates in the development of obesity-associated metabolic complications.

Recent evidence supports that AT-derived EVs play an important role in the AT secretome and its metabolic effects, leading us to characterize the adipokine profiles of lean and obese adipocyte-derived EV subtypes. We identified that adiponectin is one of the most enriched adipokines in AT-derived EVs, that it is preferentially associated with the sEV subtype, and that its content was mainly driven by nonspecific adsorption of this hormone to these nanovesicles. EVs nonetheless provide stable carriers for adiponectin delivery and maintain its insulin-sensitizing properties *in vitro* and *in vivo*. Moreover, adiponectin-associated EVs demonstrate anti-inflammatory properties that can limit macrophage tissue infiltration and are likely to participate in metabolic health improvement. Our results therefore provide a new understanding of adiponectin-related metabolic responses by highlighting EVs as delivery platforms for metabolically active forms of adiponectin molecules.

## RESULTS

### Obesity increases EV subtype secretion from fat depots

EV isolation was performed from cultured visceral adipose tissue (VAT) conditioned media using differential ultracentrifugation, namely, 13,000 × *g* for lEVs and 100,000 × *g* for sEVs. The significant EV size-distribution profiles (Figure 1A) and mean size differences (Figure 1B) observed between lEVs and sEVs were still maintained when EV subtypes were isolated from obese VAT. Higher EV concentrations, for both lEVs and sEVs, were measured when EVs were isolated from obese (*ob/ob*) VAT explant conditioned media compared to those with lean conditions (Figure 1A). A specific enrichment of flotillin-2 membranous protein was observed in lEVs, reflecting an ectosome-enriched EV subpopulation, whereas sEVs were enriched in tetraspanins (Alix, CD9, and CD63), illustrating their endolysosomal biogenesis pathway (Figure 1C). Obese VAT-derived sEVs displayed a strong enrichment in CD63 (Figures 1C and 1D). Comparison of EV secretion according to fat location revealed the common ability of VAT, subcutaneous adipose tissue (SAT), and brown adipose tissue (BAT) to secrete lEVs and sEVs, although VAT appeared to be the highest producer of EV subtypes over the other fat depots (Figure 1E). Obesity was associated with increased adipose EV secretion from VAT (Figure 1F) and SAT (Figure S1A), whereas similar EV production was measured from lean and obese BAT (Figure S1B). Measurement of EV secretion originating from human fat biopsies from obese patients confirmed the ability of VAT (i.e., omental and mesenteric fat depots) to secrete more sEVs per gram of fat in comparison to that secreted by subcutaneous AT (Figure 1G).

### Adipocyte-derived EV-adipokine profiling identifies adiponectin as an EV-abundant protein

Quantifying EVs derived from adipocytes in the circulation would require the identification of adipocyte-specific proteins specifically sorted by EVs, among which adipokines represent the main candidates. By blotting EV subpopulations isolated from conditioned media of 48-h cultured isolated adipocytes from collagenase-digested lean VAT with adipokine arrays, we found similar adipokine patterns for lEVs and sEVs and identified adiponectin and resistin as the most EV-enriched adipokines (Figures 1H and S1C). In addition, detectable amounts of dipeptidyl peptidase 4, fibroblast growth factor 1, endocan, lipocalin, intercellular adhesion molecule 1 (ICAM-1), retinol binding protein 4 (RBP4), and plasminogen activator inhibitor 1 were also present in isolated lean adipocyte-derived lEV and sEV preparations (Figures 1H and S1C). Similar adipokine EV profiles were obtained when arrays were blotted with VAT-derived EV subtypes from lean or obese (*ob/ob*) mice, confirming that a selective subset

(H) Quantification of adipokine arrays incubated with EV subpopulations isolated from conditioned media of adipocytes isolated from collagenase-digested lean VAT cultured for 48 h. Representative blotted adipokine arrays are presented in Figure S1C.

(I and J) The EV-associated adiponectin content is enriched in sEVs and is decreased with obesity. VAT-derived lEVs and sEVs (8 μg each) from lean or *ob/ob* (Ob) mice were analyzed by western blotting for the presence of adiponectin in reduced conditions (I). Blot quantification of the adiponectin signal in lean VAT-derived EV subtypes (J) reveals a particular enrichment of adiponectin in sEVs. Each color represents an independent experiment, with lEV and sEV preparations derived from the same VAT. n = 6, mean ± SEM, *p ≤ 0.05 (t test for matched pairs).

(K) Adiponectin forms detected in lean VAT-derived EVs. R and NR represent reducing or nonreducing unheated conditions, respectively. HMW, MMW, and LMW represent high, middle, and low molecular weight, respectively. One representative blot out of two independent experiments is shown.

(L) ELISA quantification of the adiponectin content of VAT-derived sEVs isolated from lean or obese VAT explants. Obese VAT-derived sEVs, isolated from either *ob/ob* (Ob) or HFD mice, are depleted of adiponectin (Adpn) compared to sEVs produced from VAT collected from their respective lean control mice (Ctrl and SD). The results are presented as box and whisker plots with the mean from four sEV independent samples measured for each condition (Ctrl, Ob, SD, and HFD).

Data are presented as the mean ± SEM for (A) to (J), dot plots representing independent samples. Statistical differences were assessed using one-way ANOVA (B, D, F), multiple t tests (E, G), or the Mann-Whitney test (L).

Statistical significance is indicated for each panel as follows : *p ≤ 0.05, **p ≤ 0.01, ***p ≤ 0.01,****p ≤ 0.0001.

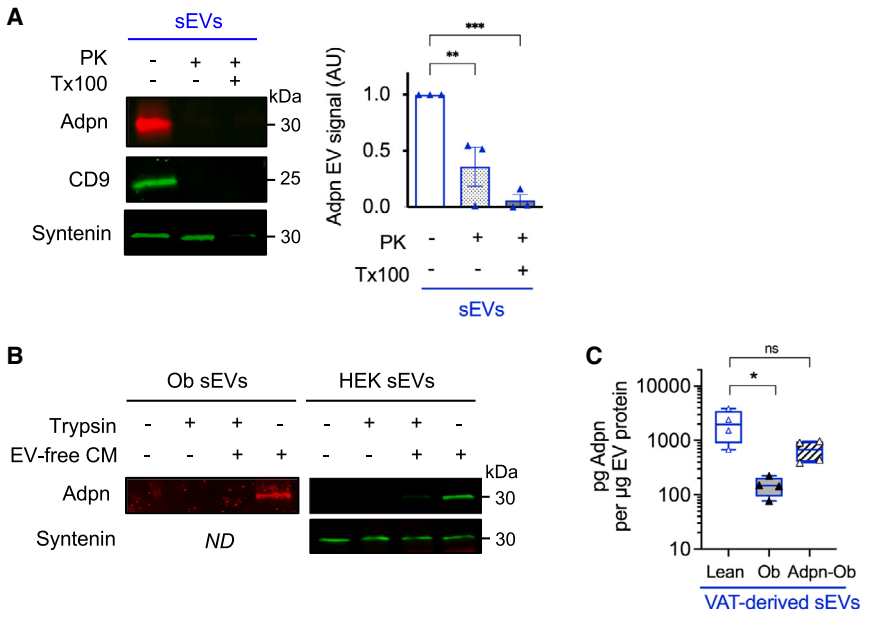


**Figure 2. Adiponectin-associated EVs preferentially distribute at the EV outer surface**

(A) The proteinase K (PK) protection assay reveals the adiponectin-associated sEV-surface pool. The transmembrane protein CD9 and internal syntenin-1 were used as positive controls for PK activity and PK/Tx100 combined activities, respectively. Blot quantification for the Adpn signal is presented on the right of the panel. n = 3, mean ± SEM, $^{**}p \leq 0.01$, $^{***}p \leq 0.001$ (one-way ANOVA).

(B) EV adiponectin surface pool adsorption depends on sEV-surface proteins. One representative blot is shown out of n = 3 for Ob sEVs and out of n = 2 for HEK sEVs. Syntenin is presented as a loading control. ND, not determined.

(C) Adiponectin adsorption on obese VAT-derived sEVs recapitulates the adiponectin EV content of lean VAT-derived sEVs. ELISA measurement of adiponectin in sEVs isolated from lean VAT (Ctrl) and obese VAT prior to (Ob) or after incubation with EV-depleted VAT conditioned medium (Adpn-Ob) that leads to sEV adiponectin adsorption (as presented in B). Data are presented as the mean ± SEM from four sEV independent samples measured for each condition (Ctrl, Ob, and Adpn-Ob), $^{*}p \leq 0.05$ (one-way ANOVA test corrected with Sidák's multiple comparisons test); ns, not significant.

of adipose secreted molecules (among those tested) are using the EV secretion pathway (Figures S1D and S1E).

Since adiponectin is one of the most abundantly expressed adipokines of AT-derived EVs and its expression is restricted to adipocytes, we next focused on the association of adiponectin with VAT-derived EV subtypes. We demonstrated its specific enrichment within sEVs in comparison to lEVs under lean conditions (Figures 1I and 1J). Under nonreducing conditions, high- and middle-molecular-weight forms of adiponectin, recognized as metabolically active forms, were particularly enriched in the sEV population (Figure 1K). When submitted to a density gradient, lEV-associated adiponectin colocalized with the lEV markers flotillin-2 and β-actin (Figure S1F), whereas sEV-associated adiponectin floated in fraction 3 enriched in CD9 and CD63 (Figure S1G). Soluble adiponectin (still present in EV-free VAT conditioned media) and sEV-associated adiponectin were retrieved in different fractions, excluding any contamination of sEV-associated adiponectin by nonvesicular adiponectin (Figure S1H). By using an immunocapture technique allowing the isolation of $CD9^{+}CD63^{+}CD81^{+}$-enriched sEVs, we further confirmed the presence of adiponectin in immunoprecipitated sEVs (Figure S1I).

EV-associated adiponectin levels dropped in obese conditions (Figures S1D and S1E), reaching undetectable levels of adiponectin protein in obese VAT-derived EVs (Figure 1I). ELISA quantification of EV-associated adiponectin demonstrated a 40-fold enrichment of lean VAT sEV adiponectin content (~1,000 pg adiponectin/µg EV protein) compared to that measured in *ob/ob* (obese) VAT-derived sEVs (Figure 1L). Obese or high-fat diet (HFD) VAT-derived sEVs were equally depleted of adiponectin compared to sEVs derived from their respective lean control mice (control [Ctrl] or standard diet [SD]), therefore excluding any confounding effect of leptin deficiency on the decreased adiponectin content of sEVs (Figure 1L).

## Adiponectin-associated EVs are mainly distributed on the EV external face

To characterize the vesicular adiponectin association, we subjected VAT-derived sEVs to a proteinase K (PK) protection assay. The majority of the sEV-associated adiponectin signal disappeared following PK treatment, illustrating the distribution of adiponectin mainly on the EV external surface (Figure 2A). We next tested the ability of EVs to stick to nonvesicular secreted adiponectin by incubating sEVs derived either from obese VAT or HEK cells (which displayed low or no adiponectin protein signal, respectively) with EV-free VAT conditioned media as a source of soluble adiponectin. We observed important adsorption of adiponectin to sEVs. This association was completely abolished when sEVs were pretreated with trypsin, highlighting the involvement of EV extracellular proteins in adiponectin binding to the EV surface, irrespective of the sEV cellular source (Figure 2B). Adiponectin levels adsorbed to obese VAT-derived sEVs did not exceed the adiponectin content of lean VAT-derived sEVs, suggesting a limitation of the number of adiponectin molecules that could stick to sEVs, likely due to steric hindrance caused by the sEV size (Figure 2C).

## EVs constitute stable conveyors of adiponectin in the blood circulation

We next tracked fluorescent VAT-derived EVs isolated from mice expressing the fluorescent protein ZsGreen specifically in adipocytes (Figures S2A and S2B). Flow-cytometry analysis identified approximately 2% $ZsGreen^{+}$ EVs in mouse plasma (Figure 3A), a percentage that might be underestimated, since the laser beam of the flow cytometer used does not resolve light scattered by particles smaller than 500 nm, therefore excluding sEV quantification. Total EV depletion from mouse plasma led to a nearly 20% drop in adiponectinemia, identifying plasma EVs as effective conveyors of adiponectin (Figure 3B). We confirmed the presence of oligomeric

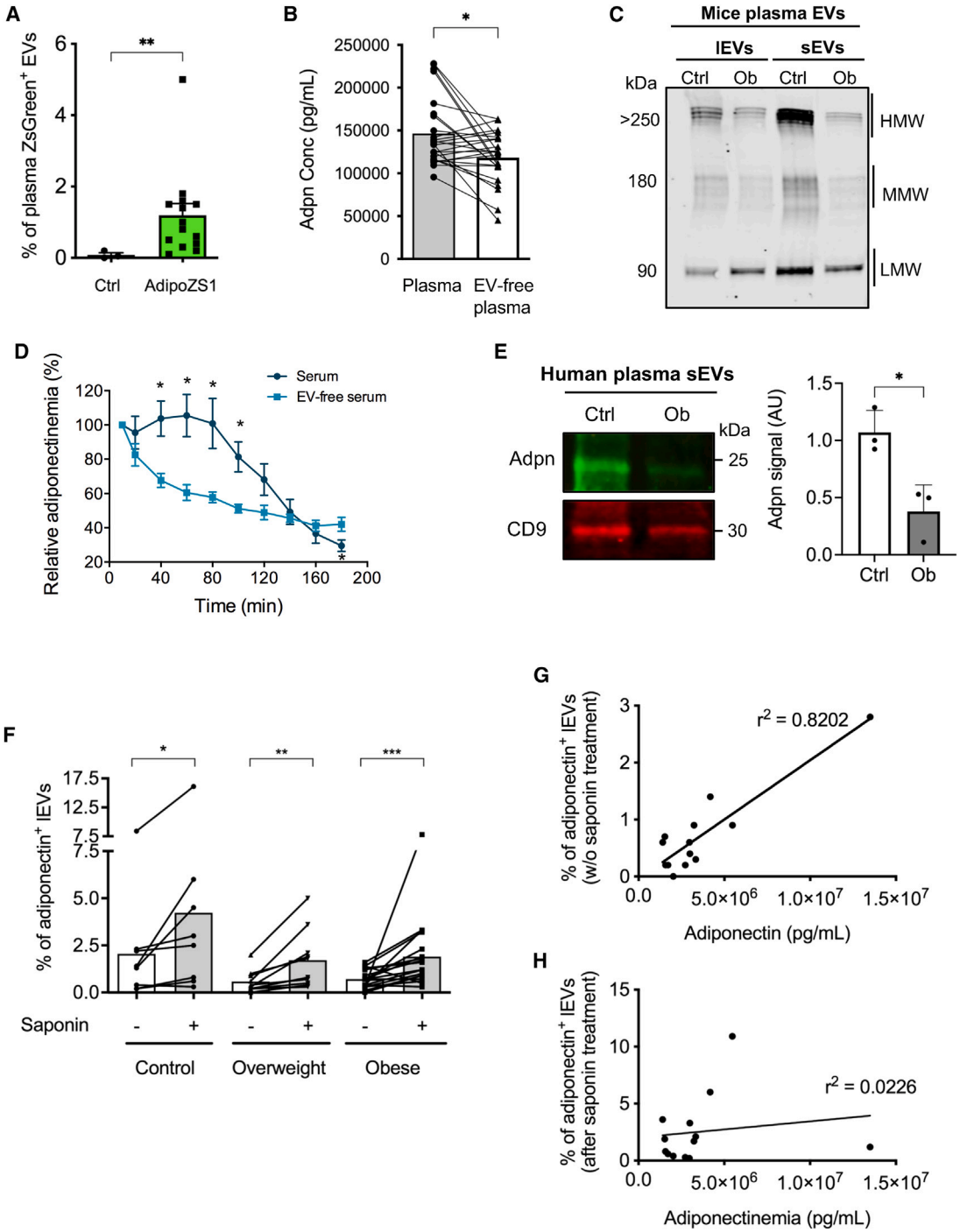


**Figure 3. Plasma EVs represent stable carriers of adiponectin**

(A) VAT-derived EVs are retrieved in the blood circulation, as illustrated by flow-cytometry detection of ZsGreen$^{+}$ EVs in platelet-free plasma (PFP). Ctrl, control; AdipoZS1, Cre$^{-}$ AdipoZs1 mice; AdipoZS1, Cre$^{+}$ AdipoZs1 mice.

(B) Adiponectinemia significantly decreases upon plasma EV removal in lean mice.

(C) The presence of adiponectin was confirmed in mouse plasma circulating EVs. Plasma EV subtypes were isolated from lean and obese mice. Ten micrograms of each EV subtype was resolved by SDS-PAGE under reducing conditions (R) or nonreducing unheated conditions (NR). One representative blot (out of two experiments performed) is presented.

(D) Adiponectin clearance measurement following the injection of serum or EV-depleted serum in adiponectin KO mice. n = 6 mice injected per group.

(E) Western blot of human plasma sEVs confirms the decreased amount of adiponectin in sEVs isolated from obese patients compared to control patients. A representative blot (out of three independent experiments performed) is presented with quantification of the Adpn blot signal intensity.

*(legend continued on next page)*

adiponectin forms in plasma EVs, mostly enriched in the sEV subpopulation, whose content dropped in obese mice following plasma adiponectin levels (Figure 3C). Similar to VAT-derived EVs, plasma EV-associated adiponectin was distributed at the external face of lEVs and sEVs, as proven by the adiponectin signal disappearance following PK treatment (Figure S2C). We next measured the clearance rate of plasma adiponectin following injection of wild-type serum (depleted or not of EVs) into the tail vein of adiponectin knockout (KO) mice. We demonstrated a drastic reduction in blood adiponectin stability in the absence of EVs, suggesting that EVs act as stable scaffolds of metabolically active forms of adiponectin in the circulation (Figure 3D).

Lastly, we explored the clinical relevance of adiponectin EV trafficking in human blood samples collected from healthy, overweight, or obese patients (Table S1). For mice, the adiponectin content detected in plasma-derived sEVs was drastically reduced in patients with obesity compared to healthy controls (Figure 3E). Adiponectin was also distributed at the external face of human plasma sEVs, although we identified a significant intravesicular pool that was degraded after Triton X-100 sEV membrane permeabilization (Figure S2D). Flow-cytometry analysis of patient platelet-free plasma demonstrated an elevation of plasma lEV concentrations in obese patients (Figure S2E). We previously reported that this elevation of circulating lEVs in obese patients was associated with a significant increase in platelet and endothelial cell-derived lEVs and a trend toward an increase in the procoagulant activity of lEVs.[11] In the absence of saponin membrane permeabilization, we identified a small portion (~2.5%) of adiponectin$^+$ plasma lEVs in control healthy patients that dropped and was close to background in overweight and obese patients (Figure 3F, white bars), therefore paralleling the drop in plasma adiponectin levels during obesity (Table S1). Accordingly, adiponectin$^+$ lEV levels measured in the absence of saponin strongly correlated with plasma adiponectinemia measured in the same patients (Figure 3G). In addition, saponin treatment significantly increased the adiponectin positivity of lEVs in all patient groups, revealing a second pool of adiponectin enclosed within the vesicles (Figure 3F, gray bars) that was not associated with plasma adiponectin levels (Figure 3H). Despite evidence that large plasma EVs (over 500 nm in diameter according to the flow cytometer lower detection limit) display both external and intravesicular adiponectin-associated EV pools, we cannot exclude the possibility that saponin treatment may also favor unfolding and/or unmasking of adiponectin antigens, thereby contributing to increased adiponectin-positive EV signals and overestimating the adiponectin intravesicular pool.

Altogether, our results demonstrate that EVs definitely convey adiponectin, but the unspecific adsorption, which is closely related to patient adiponectinemia, precludes their use for the quantification of adipocyte-derived EVs.

## Adiponectin-associated sEVs mediate insulin-sensitizing effects in target cells

Adiponectin is recognized as an insulin-sensitizing hormone that signals on target tissues, such as the liver and skeletal muscle, mainly via the adiponectin receptors AdipoR1 and AdipoR2. Treatment of hepatocytes rendered insulin resistant following palmitate exposure with 5 μg/mL lean VAT-derived sEVs was sufficient to fully restore insulin-induced AKT phosphorylation, suggesting that the high adiponectin content of these sEVs mediates these insulin-sensitizing effects (Figure 4A). In contrast, obese VAT-derived sEVs failed to restore palmitate-treated HepG2 insulin sensitivity, whereas *in vitro* enrichment of these obese sEVs with adiponectin fully counteracted insulin resistance (Figure 4B). We next questioned whether adiponectin-associated sEV insulin-sensitizing effects involved the two canonical receptors by knocking down AdipoR1 and AdipoR2 in HepG2 cells (Figure S3A). Silencing of both these receptors abolished the reversal of HepG2 insulin resistance by lean VAT-derived sEVs, further demonstrating that the insulin-sensitizing properties of adipose sEVs are linked to the presence of adiponectin on these vesicles and identifying vesicular adiponectin binding to AdipoR as a critical step in sEV-induced insulin-sensitizing action (Figure 4C). Adiponectin is likely not the sole molecule that varies in VAT-secreted EVs according to lean or obese status. Moreover, the adipose origin of sEVs will determine the innate EV biocorona (containing membrane integral and peripheral constituents), which is emerging as a critical mediator of EV functions.[26] To study the impact of the cellular origin of EVs on adiponectin-enriched sEV beneficial effects, we switched to naive HEK293 cells that do not express endogenous adiponectin, in which we overexpressed either a fluorescent-tagged adiponectin-Venus (Adpn-Venus) or the Venus tag alone (Figures S3B and S3C). Small EVs carrying either the Venus tag or Adpn-Venus were further isolated from the respective stable HEK293 cell line conditioned media (Figure S3D). HEK293-derived Adpn-Venus sEVs can readily and efficiently target HepG2 cells, as demonstrated by their rapid and time-dependent hepatocyte internalization (Figure 4D). Adpn-Venus sEVs reversed the insulin resistance of palmitate-treated hepatocytes, firmly establishing the critical role of vesicular adiponectin in the insulin-sensitizing effects of lean VAT-derived sEVs, independent of the sEV cellular origin (Figure 4E). The insulin-sensitizing effects of Adpn-Venus were strongly reduced by the silencing of both AdipoR1 and AdipoR2 (Figure 4E).

Collectively, our results demonstrate that adiponectin-associated EVs display the same insulin-sensitizing properties as those described for soluble adiponectin (for review, see Straub and Scherer[4]), which occur through binding to

(F) Analysis of adiponectin positivity of human plasma lEVs by flow-cytometry analysis. Percentage of adiponectin$^+$ lEVs retrieved in plasma in patients before (white bars) and after (gray bars) saponin permeabilization is presented for control (BMI $\leq$ 27), overweight (27 < BMI $\leq$ 30), and obese (BMI >30) patients.
(G and H) Linear regression between adiponectinemia and adiponectin$^+$ lEV rates measured for patients in the absence (G) or presence of (H) saponin.
Data are presented as the mean ± SEM, dot plots representing independent experiments. The connected lines identify the same sample analyzed before/after EV depletion (for B) or saponin treatment (for F). Statistical differences were assessed using the Mann-Whitney test (A, B, E), multiple t tests (D), and the Wilcoxon matched-pairs signed rank test (F).
Statistical significance is indicated for each panel as follows : *p $\leq$ 0.05, **p $\leq$ 0.01, ***p $\leq$ 0.01,****p $\leq$ 0.0001.

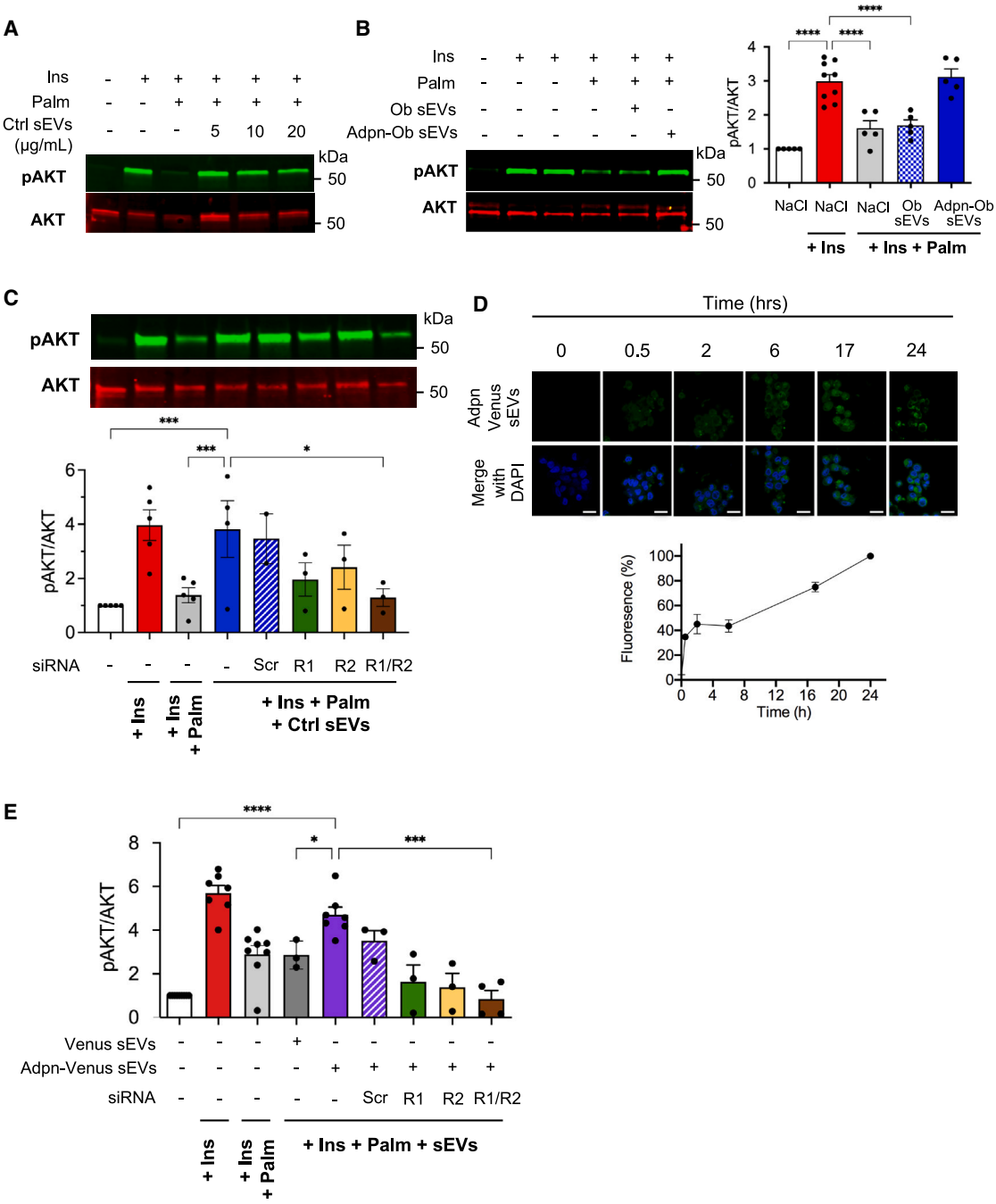


**Figure 4. EV-associated adiponectin maintains insulin sensitivity in target cells**

(A and B) Adiponectin-enriched sEVs reverse insulin resistance in hepatocytes. Ctrl sEVs and Ob sEVs correspond to VAT-derived sEVs isolated from either lean or obese VAT, respectively. Adpn-Ob sEVs refer to the enrichment of Ob sEVs with adiponectin (following their preincubation with EV-free conditioned media). Ins, insulin; Palm, palmitate.

(C) Silencing of both AdipoR1 and AdipoR2 significantly reduces the VAT-derived sEV insulin-sensitizing effects. Scr, Scramble; R1, AdipoR1; R2, AdipoR2.

(D) Rapid and time-dependent internalization of fluorescent adiponectin-Venus (Adpn-Venus) internalization in hepatocytes. Scale bars, 50 µm.

(E) Adiponectin enrichment in sEVs is responsible for their insulin-sensitizing effects, independent of their sEV cellular origin.

Dot plots represent independent experiments. Data are presented as the mean ± SEM. Statistical differences were assessed using one-way ANOVA. Statistical significancy is indicated for each panel as follows : *p ≤ 0.05, **p ≤ 0.01, ***p ≤ 0.01,****p ≤ 0.0001.

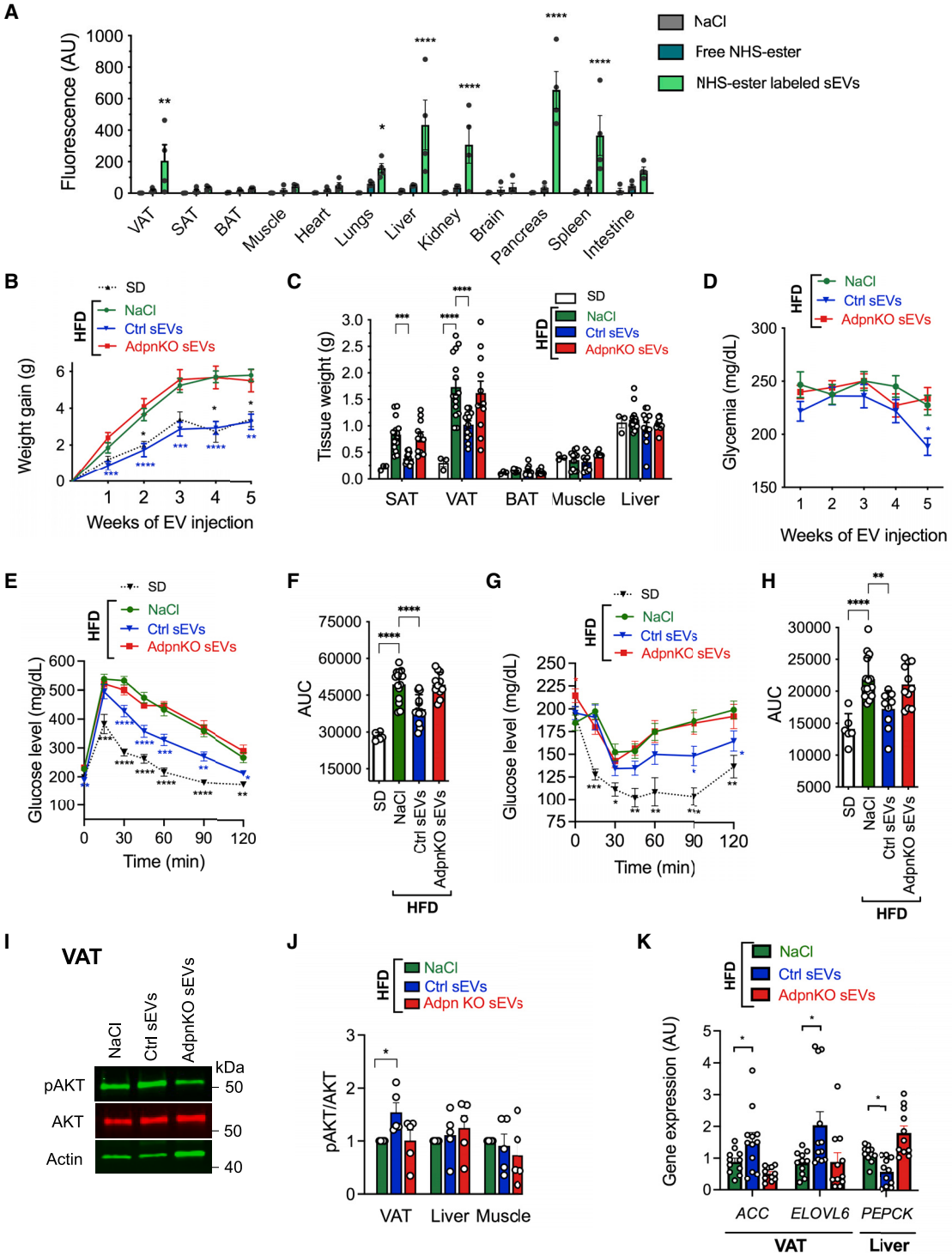


**Figure 5. EV-associated adiponectin reverses HFD-induced insulin resistance in mice**

(A) NHS ester-labeled VAT-derived sEV organ biodistribution. Licor fluorescent tissue imaging is presented in Figure S4A.

(B) Adoptive transfer of sEV-associated adiponectin limits weight gain induced by a high-fat diet (HFD). A standard diet (SD) is presented as a control to demonstrate HFD-induced weight gain compared to body weight on a regular chow diet. Number of animals per group: SD, n = 3; NaCl, n = 15; Ctrl sEVs, n = 13; AdpnKO sEVs, n = 11.

(C) Tissue weights at sacrifice of mice that received i.p. injections of Ctrl sEVs, AdpnKO sEVs, or NaCl (vehicle) over the course of 5 weeks of HFD compared to mice maintained on an SD.

*(legend continued on next page)*

regular adiponectin receptors and downstream signaling cascades.

### Adiponectin-associated sEVs improve mouse glucose homeostasis *in vivo* by exerting insulin-sensitizing effects on VAT and liver

We next questioned the ability of adiponectin-enriched sEVs to mediate insulin-sensitizing effects *in vivo*. The biodistribution of *N*-hydroxysuccinimide (NHS) ester covalently labeled sEVs identified vascularized tissues such as the lungs, liver, kidney, pancreas, and spleen as the sEV main targets, as is commonly reported for the EV biodistribution regardless of the EV administration.[27] Importantly, we also detected significant fluorescent sEV signals in VAT depots (Figures 5A and S4A). Nonetheless, we cannot exclude the possibility that the sEV labeling, involving the reaction of the NHS ester amine-reactive group with the primary amines of proteins, impacts the sEV protein structure and, thereby, sEV targeting.

We then performed adoptive transfer of lean VAT through repetitive intraperitoneal (i.p.) EV injections in mice fed an HFD over 5 weeks to mimic physiological VAT-derived EV diffusion. We first highlighted the specific ability of lean VAT-derived sEVs to significantly improve the glucose tolerance of obese mice in comparison to lean VAT-derived lEV or NaCl (vehicle) injections, arguing favorably for a role of adiponectin specifically enriched in sEVs in these beneficial effects (Figures S4B and S4C). To delineate the role of adiponectin-associated sEVs in the insulin-sensitizing effects, we next compared the effects of adoptive transfer of lean VAT-derived sEVs (Ctrl) that are enriched in adiponectin with those of VAT-derived sEVs from adiponectin KO (AdpnKO) mice or vehicle (NaCl)-treated mice during the course of HFD feeding. Ctrl sEV-injected mice were protected against HFD-induced weight gain compared to NaCl or AdpnKO sEV injections and overlapped with the body-weight-gain curve of the SD-fed mouse group (Figure 5B). Consequently, control sEV-treated animals were leaner (Figure S4D) and displayed lower adiposity (Figure S4E). A significant decrease in both visceral and subcutaneous AT depots was measured in adiponectin-enriched sEV-injected animals, whereas the BAT, muscle, and liver total weights remained unchanged (Figure 5C). This reduced fat storage capacity was associated with a significant shift in the adipocyte size-distribution curve toward smaller adipocyte diameters specifically observed for adiponectin-enriched (Ctrl) sEV-treated mice in both VAT and SAT (Figures S4F and S4G). All mouse groups displayed similar food intake as well as unchanged mRNA expression of key thermogenic genes in BAT and SAT (Figures S4H and S4I). Moreover, control sEV treatment was associated with whole-body glucose improvement, as illustrated by significantly reduced fasting glycemia over the course of HFD compared to NaCl-injected or AdpnKO sEV-injected mice (Figure 5D). Accordingly, adiponectin-associated sEVs specifically improved glucose tolerance compared to NaCl or AdpnKO sEV injections (Figures 5E and 5F). A better insulin sensitivity of adiponectin-enriched sEV-treated mice was also observed as measured by the insulin tolerance test (Figures 5G and 5H). This improvement in glucose homeostasis was accompanied by enhanced insulin-stimulated AKT phosphorylation specifically in VAT (Figures 5I and 5J), whereas no significant changes in the phospho-AKT/AKT ratio in response to insulin were measured in liver or muscle (Figure 5J). We measured the mRNA levels of well-known insulin targets in the VAT and reported a specific increase in the mRNA expression of acetyl-coenzyme A carboxylase and elongation of long-chain fatty acid family member 6 in Ctrl sEV-injected mice (Figure 5K). In the liver, we observed a significant downregulation of the mRNA levels of the gluconeogenic gene phosphoenolpyruvate carboxykinase (PEPCK) following Ctrl sEV injections (Figure 5K).

We next performed histological examinations of muscle and liver samples to evaluate ectopic fat tissue deposition under HFD challenge. Skeletal muscle cross-section staining did not reveal either muscle fiber injury or aberrant lipid deposition under HFD conditions within each group (Figure S4J). Conversely, sEV injections prevented the development of hepatic steatosis, which was observed in both vehicle (NaCl)- and AdpnKO sEV-treated mice fed an HFD (Figure S4J). Accordingly, a significant reduction in hepatic peroxisome proliferator-activated receptor $\gamma$ (PPAR$\gamma$) mRNA expression was observed in adiponectin-associated sEV-treated animals (Figure S4K). Finally, we investigated liver function by measuring circulating markers of liver function such as the serum concentrations of hepatic transaminases (Table 1). We observed that AdpnKO sEVs induced a significant increase in the serum aspartate aminotransferase concentration, highlighting the induction of hepatic damage by sEVs devoid of adiponectin (Table 1), thereby further underlining the protective role played by adiponectin-associated sEVs against liver injury.

Altogether, we demonstrated significant improvement in glucose homeostasis following the injection of adiponectin-enriched sEVs, with major effects occurring in the VAT and liver, illustrating the conserved insulin-sensitizing properties of vesicular forms of adiponectin *in vivo*.

(D) Glycemia was measured following a 4-h fast performed prior to EV injection. Number of animals per group: NaCl, n = 15; Ctrl sEVs, n = 13; AdpnKO sEVs, n = 11.

(E–H) Metabolic tolerance tests were performed to assess glucose homeostasis metabolism. Intraperitoneal glucose tolerance tests (GTTs) (E) and insulin tolerance tests (ITTs) (H) are presented where blood glucose was quantified at the indicated time points after glucose or insulin injection, respectively. The area under the curve (AUC) for the GTT is presented in (F). Circulating insulin (G) was measured 15 min post glucose injection during the GTT. Number of animals per group: SD, n = 6; NaCl, n = 15; Ctrl sEVs, n = 13; AdpnKO sEVs, n = 11.

(I and J) Western blot analysis of AKT phosphorylation (Ser473) levels in VAT after mouse insulin injection (I). Quantification of the phospho-AKT (Ser473)/AKT ratio (pAKT/AKT) in VAT, liver, and muscle tissues after mouse insulin injection is presented in (J).

(K) mRNA expression of key metabolic genes known to be transcriptionally regulated by insulin in VAT or liver.

Dot plots represent the number of independent animals analyzed. Data are presented as the mean ± SEM. Statistical differences were calculated compared to the HFD + NaCl group using one-way ANOVA followed by the Kruskal-Wallis test (A, C, F, G, J, K) and repeated-measures ANOVA followed by the Holm-Sidák test for multiple comparisons (B, D, E, H).

Statistical significance is indicated for each panel as follows : *p $\leq$ 0.05, **p $\leq$ 0.01, ***p $\leq$ 0.01,****p $\leq$ 0.0001.

**Table 1. Serum liver metabolic parameters in mice**

| | SD | | | | HFD | | | | | | | | | | | |
|---|---|---|---|---|---|---|---|---|---|---|---|---|---|---|---|---|
| | | | | | NaCl | | | | Ctrl sEVs | | | | AdpnKO sEVs | | | |
| | Mean | SEM | n | p | Mean | SEM | n | p | Mean | SEM | n | p | Mean | SEM | n | p |
| Total cholesterol (mg/dL) | 110.7 | 8.5 | 3.0 | 0.064 | 232.2 | 48.7 | 7.0 | | 165.1 | 23.4 | 7.0 | | 227.4 | 13.6 | 7.0 | |
| Total protein (g/dL) | 4.8 | 0.3 | 3.0 | | 5.8 | 1.0 | 7.0 | | 5.6 | 0.7 | 7.0 | | 6.2 | 0.4 | 7.0 | |
| Albumin (g/dL) | 2.7 | 0.1 | 3.0 | | 3.2 | 0.5 | 7.0 | | 2.9 | 0.3 | 7.0 | | 3.1 | 0.2 | 7.0 | |
| Globulin (g/dL) | 2.1 | 0.2 | 3.0 | | 2.6 | 0.4 | 7.0 | | 2.7 | 0.4 | 7.0 | | 3.1 | 0.3 | 7.0 | |
| ALT (U/L) | 94.0 | 16.0 | 3.0 | | 576.3 | 224.1 | 6.0 | | 324.3 | 114.5 | 7.0 | | 811.1 | 329.2 | 7.0 | |
| AST (U/L) | 222.0 | 55.2 | 3.0 | | 333.4 | 74.4 | 7.0 | | 450.3 | 146.3 | 7.0 | | 1,020.2* | 295.2 | 7.0 | 0.048 |
| ALP (U/L) | 128.0 | 19.1 | 3.0 | | 96.9 | 7.5 | 7.0 | | 70.0 | 4.3 | 7.0 | | 71.2 | 13.4 | 6.0 | |
| Bilirubin (mg/dL) | 0.2 | 0.0 | 3.0 | | 0.4 | 0.2 | 7.0 | | 1.0 | 0.3 | 7.0 | | 0.6 | 0.3 | 7.0 | |

Data are presented as the mean ± SEM. Statistical differences were assessed using one-way ANOVA. *$p \leq 0.05$ indicates a statistical significance between HFD NaCl and HFD AdpnKO sEVs conditions. ALT, alanine aminotransferase; AST, aspartate aminotransferase; ALP, alkaline phosphatase.

### Adiponectin-associated sEVs reduce HFD-induced tissue inflammation

In addition to the well-documented insulin-sensitizing potential of adiponectin, experimental evidence has also demonstrated the anti-inflammatory effects of this adipokine (for review, see Fantuzzi[28]). Since inflammation is recognized as a major contributor to insulin resistance in the context of obesity, we aimed to investigate the effects of adiponectin-associated sEVs on inflammation markers in EV-metabolism-targeted tissues. By first focusing on adipose depots, we demonstrated histological hallmarks of adipose macrophage infiltration in both the SAT and VAT of HFD animals treated with NaCl or AdpnKO sEV injections, as illustrated by the presence of macrophage ($Mac2^+$) crown-like structures (Figure 6A). Of note, such structures were absent in AT depots from control sEV-injected mice (Figure 6A). The anti-inflammatory action of adiponectin-associated sEVs was further confirmed by a significant reduction in the mRNA expression of the proinflammatory factors interleukin-6 (IL-6) and monocyte chemoattractant protein 1 (MCP-1) in the VAT of Ctrl sEV-injected mice (Figure 6B). Conversely, AdpnKO sEV injections further enhanced HFD-associated VAT inflammation compared to NaCl injections, as illustrated by the significant increase in IL-1β and tumor necrosis factor α (TNF-α) mRNA expression, two proinflammatory cytokines known to be largely produced by macrophages (Figure 6B). Similar to what was observed in VAT, control sEVs also resolved liver inflammation, likely by limiting macrophage infiltration, as illustrated by the significant reduction in the chemoattractant cytokine MCP-1 mRNA expression compared to that in NaCl conditions (Figure 6C). Alternatively, sEVs devoid of adiponectin injections contributed to enhanced liver inflammation, as revealed by the significant increase in hepatic IL-1β and TNF-α mRNA expression over NaCl conditions (Figure 6C). These results suggest that the presence of adiponectin in sEVs controls tissue macrophage recruitment in both VAT and liver (Figures 6B and 6C).

Thus, the presence of adiponectin in sEVs displays potent anti-inflammatory properties that likely contribute to mediating its insulin-sensitizing effect.

## DISCUSSION

We identified adiponectin as one of the most enriched adipokines in adipocyte-derived EVs, whose content was mainly driven by its nonspecific adsorption to these nanovesicles. EVs nonetheless serve as stable carriers for adiponectin delivery that display both insulin-sensitizing and anti-inflammatory properties.

We confirmed the AT capacity to secrete both lEVs and sEVs, whose secretion was enhanced in the obesity context, as previously demonstrated for sEVs.[18,19] Whereas obesity did not impact EV subtype size, we revealed CD63 enrichment in obese VAT-derived sEVs, in agreement with previous data reporting high levels of CD63 in HFD mature adipocyte-derived sEVs.[29] CD63 has been shown to be abundantly enriched in exosomes (even if not exclusively) in comparison to other tetraspanins, such as CD9 or CD81, and to traffic via acidic compartments.[30] Different studies have noted altered expression of lysosomal membrane proteins (such as cathepsins) in obese AT that consequently reduces lysosomal acidity.[31] Such lysosomal dysfunction may explain the selective enhancement of the sEV-dependent CD63 secretion pathway derived from endolysosomal compartments in obese conditions. A recent study also demonstrated that EV surface CD63 expression is associated with obesity-related traits such as waist circumference, in agreement with a close relationship between $EV^{CD63+}$ and obesity.[32]

We moreover highlighted VAT, in both mice and humans, as providing a greater abundance of EVs than subcutaneous AT depots. This higher secretion ability may be linked to adipocyte size, since VAT adipocytes are more hypertrophied than subcutaneous adipocytes. VAT is also known to be more susceptible to metabolic alterations associated with chronic obesity, including hypoxia, inflammation, or lipotoxic lipid influx, which are stimuli that have all been described to induce adipocyte EV secretion.[15–17] A recent study demonstrated distinct protein contents between sEVs isolated from human obese VAT or SAT, characterized by a particular enrichment of proteins implicated in inflammation or insulin resistance in sEVs from VAT.[33]

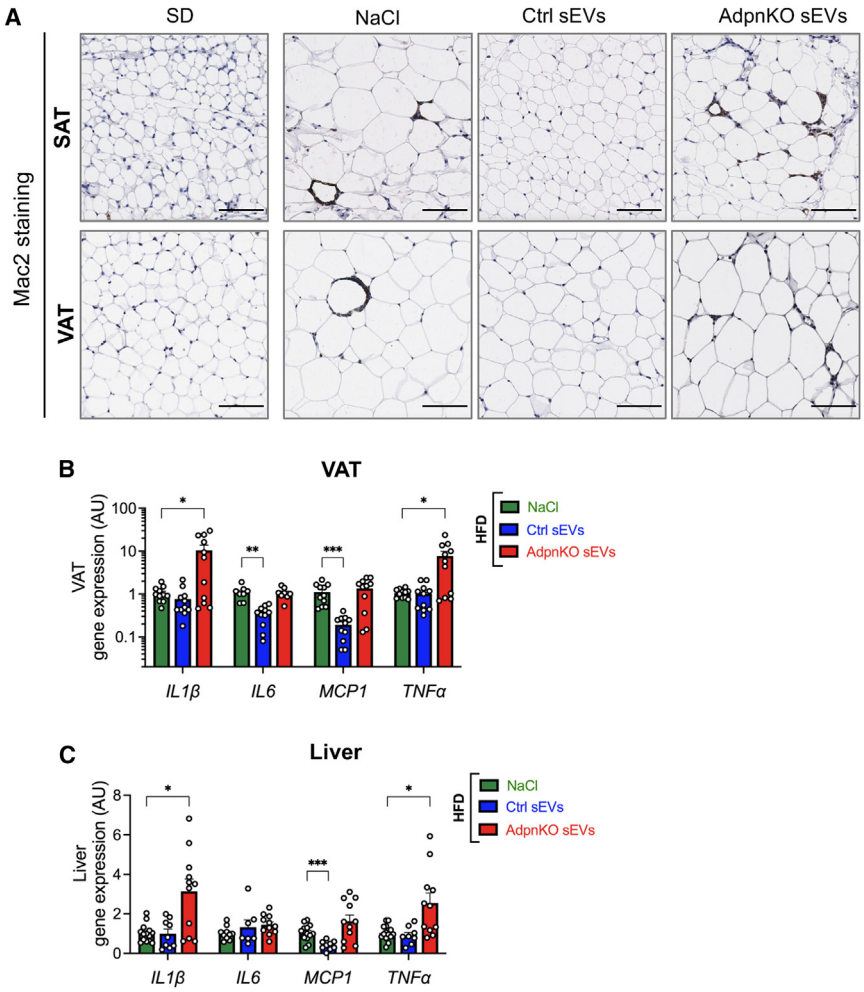


**Figure 6. EV-associated adiponectin displays anti-inflammatory properties**

(A) Macrophage (Mac2) staining in SAT (upper panels) and VAT (lower panels) depots from sEV-injected mice reveal the anti-inflammatory properties of Ctrl sEVs treatment. HFD-induced adipocyte hypertrophy and HFD-related macrophage infiltration are observed in both SAT and VAT compared to SD-fed conditions. Scale bars, 50 μm.

(B and C) qPCR mRNA expression of inflammatory markers in VAT (B) and liver (C) tissues. Dot plots represent the number of independent animals analyzed. Data are presented as the mean ± SEM. Statistical differences were calculated compared to the HFD + NaCl group using one-way ANOVA followed by the Kruskal-Wallis test.

Statistical significancy is indicated for each panel as follows : *p ≤ 0.05, **p ≤ 0.01, ***p ≤ 0.01,****p ≤ 0.0001.

Altogether, these data reinforce the idea that adipose VAT-derived sEVs could actively participate in visceral obesity-associated cardiometabolic complications.

In this regard, the identification of a specific marker of adipocyte-derived EVs to trace and quantify them in the blood would be of particular interest. Among the adipokine signatures retrieved from VAT-derived EVs, adiponectin is the sole hormone to be recognized as being specifically secreted by adipocytes. We detected neither leptin nor IL-6 or TNF-α in adipocyte-derived EVs, suggesting that adipokine EV sorting is controlled by specific mechanisms. We also identified traces of RBP4, a protein previously retrieved from obese AT-derived sEVs that has been suggested to participate in the induction of macrophage activation-induced insulin resistance.[18] We confirmed the adiponectin association with VAT-derived EVs and circulating EVs, mainly distributed at the EV outer membrane, as also demonstrated by others for serum adiponectin-associated sEVs.[34,35] Such adiponectin EV adsorption is in line with the recent interest gained by the EV (protein) corona, which appeared to be highly dependent on the biological environment and emerged as a crucial mediator of EV functions and mechanisms of cellular uptake.[36,37] Although in the minority, an intravesicular pool of adiponectin was still detectable following EV external enzymatic treatment. Recent data have shown the ability of adiponectin to stimulate, through T-cadherin binding, endothelial sEV production and resecretion of adiponectin as an exosomal cargo, contributing to a significant increase in the adiponectin circulating pool.[38] Such selective adiponectin EV sorting could account for the intravesicular presence of the adipokine. Moreover, we demonstrated that external adiponectin-associated EVs occur by nonspecific adhesion. Notably, sEVs are specifically enriched in extracellular matrix proteins when compared to the lEV subpopulation, which may explain their higher capacity to bind adiponectin.[15,39] In agreement with adiponectin adsorption on EVs, the adiponectin content in EVs fully parallels adiponectinemia. Since vesicular adiponectin adsorption is not restricted to EVs of adipocyte origin, any conclusions based on identifying circulating adipocyte-derived EVs with quantitative assays of this adipokine will lack reliability and robustness. Moreover, the external and intravesicular adiponectin pools are likely to be dependent on patient adiponectinemia and sex, since females are known to present higher circulating adiponectin levels than males.[40] This aspect will require dedicated studies to fully quantify the vesicular adiponectin pool distribution.

Previous reports have demonstrated that lean AT macrophage-derived sEV transfer into HFD recipient mice improved insulin sensitivity, an ability that was linked to macrophage-derived EV miRNA produced in the lean state.[20,41] Similarly, we demonstrated the beneficial effects of lean VAT-derived sEV injections on glucose homeostasis in HFD recipient mice, which were dependent on the presence of adiponectin-associated sEVs and were characterized by improved animal insulin sensitivity. Our EV biodistribution experiments of VAT-derived

sEVs, in agreement with a recent fluorescence adipocyte-derived sEV tracing study,[42] highlighted an important accumulation of EVs in the liver and VAT 24 h after i.p. EV injection (together with the gallbladder, pancreas, spleen, and kidney). This is consistent with the beneficial effect of adiponectin-enriched sEV injection reported in VAT and in the liver. In VAT, we reported an improvement in AKT phosphorylation upon insulin treatment and the restoration of lipogenic genes that are well known to be insulin targets. This result is of particular interest, as recent inducible deletion of adiponectin demonstrated its fundamental autocrine protective effect on AT properties and homeostasis.[43] In the liver, despite no improvement in AKT phosphorylation, we observed a decrease in the mRNA levels of PEPCK, suggesting an improvement in the ability of insulin to repress gluconeogenesis. In addition, sEV injection largely suppressed liver steatosis. Finally, adipocyte/adipose sEVs display pancreatic tropism (our results and Kulaj et al.[42]), which might also improve pancreatic β cell function. These findings are even more interesting, since adipocyte sEVs have been shown to modulate the secretion of insulin through the transport of insulinotropic cargoes[42] and because adiponectin can protect against pancreatic β cell apoptosis and increase insulin gene expression and secretion.[44] Further experiments will, however, be needed to determine the contribution of the improvement in β cell function in the global adiponectin-enriched sEV beneficial metabolism observed in treated mice.

In addition to metabolic tissues, patrolling macrophages have also been shown to be the main target cells of circulating EVs based on live tracking EV imaging.[45,46] Moreover, AT macrophages ($CD11b^+/F4/80^+$), among other AT SVF cells, take up important quantities of adipocyte-derived sEVs.[23] We demonstrated that adiponectin-enriched sEV treatment protects AT and liver from HFD-induced macrophage infiltration and thereby counteracts the massive expression of IL-1β and TNF-α, two cytokines that are considered major drivers of obesity-related insulin resistance, induced by AdpnKO sEV injections.[47,48] Our results are thus in line with a recent report demonstrating a critical role of adiponectin in preventing inflammation and macrophage infiltration in the liver.[49] While there is no conclusive information regarding whether inflammation is a cause or a consequence of insulin resistance, it is commonly accepted that both mechanisms are intrinsically linked and exacerbate each other. Therefore, the anti-inflammatory properties of adiponectin-associated sEVs are likely involved in the improvement in glucose homeostasis and global metabolic health in treated mice. Although we demonstrated the requirement of AdipoR receptors in the insulin-sensitizing effects of Ctrl sEVs on insulin-resistant hepatocytes *in vitro*, their involvement in the beneficial effects observed *in vivo* needs to be firmly established. Regarding the diversity of downstream effectors relaying adiponectin pleiotropic effects that include sphingolipid targets, AMPK, PPARα, PPARγ, and additional components (for review, see Ruan and Dong[50]), further dedicated studies are needed to decipher to what extent the adiponectin-associated sEV-induced molecular mechanisms would parallel those mediated by (soluble) adiponectin.

EVs have recently appeared as novel candidates for drug-delivery systems with high bioavailability, exceptional biocompatibility, and low immunogenicity.[51] EV-based delivery of bioactive natural adiponectin forms therefore represents an innovative therapeutic perspective to counteract both the difficulties encountered in the bioproduction of adiponectin native oligomerized forms with post-translational modifications and the short half-life of soluble adiponectin.[52] In addition to their natural abilities to cross biological barriers and interact with cells, thereby modulating target cell responses, EVs have shown some immunomodulatory and regenerative activities, holding exciting promise as therapeutic vectors.[51]

Engineered EVs displaying traceable adiponectin, targeted either inside or outside EVs, would constitute excellent tools to delineate the metabolic properties of EV-associated adiponectin with respect to adiponectin localization. Such a perspective is even more appealing in light of recent studies that formerly demonstrated the ability of EVs to deliver a protein to the cytosol of recipient cells.[53,54] Of note, such EV-based intercellular protein exchange has been evidenced within the AT, as illustrated by the ability of caveolin-1 (Cav-1)-enriched endothelial cell-derived EVs to replenish Cav-1-KO adipocytes.[23] Future studies will be needed to finely control the EV adiponectin content and compare adiponectin-associated EV biological modalities with soluble adiponectin or adiponectin receptor agonists to fully define the therapeutic potential of EV-based adiponectin therapeutic approaches.

Altogether, our results therefore provide an understanding of adiponectin-related metabolic responses by highlighting EVs as stable scaffolds of molecular active forms of adiponectin. Our results provide EV-based therapeutic perspectives for adiponectin delivery, which might be promising for the treatment of diabetes developed by lipodystrophic or obese patients.

### Limitations of the study

Our experiments demonstrating the beneficial properties of adiponectin-enriched sEVs do not allow us to fully assess either the relative quantity of adiponectin distributed between the intravesicular or the external-associated EV pool or their respective related biological effects. Moreover, we did not compare the effects of (soluble) recombinant adiponectin with those displayed by (vesicular) adiponectin-associated sEVs.

## STAR★METHODS

Detailed methods are provided in the online version of this paper and include the following:

- KEY RESOURCES TABLE
- RESOURCE AVAILABILITY
  - Lead contact
  - Materials availability
  - Data and code availability
- EXPERIMENTAL MODEL AND SUBJECT DETAILS
  - Human studies
  - Animal experimentation and *in vivo* EV treatment
- METHOD DETAILS
  - Measurement of serum liver metabolic parameters
  - Metabolic tolerance test
  - Insulin-stimulated AKT phosphorylation assay

- Primary adipocytes and adipose tissue explant culture
- AT-derived EV isolation
- Plasma/serum EV isolation
- ELISA adiponectin measurement
- Adiponectin clearance
- Mouse EV biodistribution
- EV enzymatic assays
- Cell culture
- Western blot
- Reverse transcription (RT)–quantitative PCR (qPCR)
- Nanoparticle tracking analysis (NTA)
- sEV immunocapture
- Protein arrays
- Flow cytometry assays
- Histology and immunostaining

● QUANTIFICATION AND STATISTICAL ANALYSIS

## SUPPLEMENTAL INFORMATION

Supplemental information can be found online at https://doi.org/10.1016/j.celrep.2023.112866.

## ACKNOWLEDGMENTS

We thank Prof. Weiping Han (Laboratory of Metabolic Medicine, Singapore Bioimaging Consortium) for providing the Venus-adiponectin lentiviral plasmid. We thank M. Wertheimer for technical assistance with plasmid purification. We thank Q. Massicot (SFR ICAT, Université Angers) for histological section processing. We thank the staff of Centre Hospitalier Universitaire d'Angers for analysis of clinical data of the Numevox cohort. We thank J.-C. Gimel (INSERM U1066, MINT Team, Angers, France) for providing access to nanoparticle tracking analysis technology and R. Soleti (CRCI2NA - UMR INSERM 1307 CNRS 6075, Team 4, Université Angers) for helpful comments and assistance in the redaction of animal experimentation protocols and authorizations. We thank Dr. N. Blanchard (INSERM U1291, Toulouse, France) for providing the ZsGreen1 mouse line. We thank the SCIAM imagery platform, especially F. Manero, for electron microscopy imaging and technical assistance. We also thank the PACeM platform, especially L. Bonneau and J. Cayon, for qRT-PCR experiments and C. Guillet for helpful technical assistance with flow-cytometry experiments. We thank the SCAHU platform for mouse housing and technical assistance for animal functional exploration. We acknowledge the IBISA MicroPICell facility (Biogenouest), a member of the national infrastructure France-Bioimaging supported by the French National Research Agency (ANR-10-INBS-04). We also acknowledge the THERASSAY core facility (SFR Bonamy, UMR 1087, Nantes, France) of the Scientific Interest Group (GIS) Biogenouest and IBISA for the use of the clinical chemistry analyzer Element RC. This work has been supported by grants from Genavie, Société Francophone du Diabète and the FFRD (sponsored by Fédération Française des Diabétiques, Abbott, AstraZeneca, Eli Lilly, Merck Sharp & Dohme, and Novo Nordisk), and the French National Research Agency (ANR-22-CE18-0026-02 EVADIPO). J.A. and M.D. were recipients of a doctoral fellowship from the French Ministry of Education and Research. A.B. was a recipient of a doctoral fellowship co-financed by INSERM/Région Pays de La Loire. The graphical abstract was created with BioRender.com.

## AUTHOR CONTRIBUTIONS

Methodology, A.B., J.A., J.F., G.H., M.D., and S.L.L.; experimentation and analysis, A.B., J.A., J.F., V.G., G.H., M.D., L.F., J.C., S.B., L.V., C.D., J.-P.P., and S.L.L; patient recruitment, J.D., P.-H.D., J.B., and S.D.; writing – original draft, A.B. and S.L.L.; writing –review and editing, A.B., J.A., G.H., M.D., X.P., L.V., C.D., J.-P.P., J.D., P.-H.D., S.D., J.B., B.C., and S.L.L.; conceptualization, A.B., J.A., and S.L.L.; supervision, project administration, and funding acquisition, S.L.L. All authors have read and agreed to the published version of the manuscript. S.L.L. is the guarantor of this work and, as such, had full access to all the data in the study and takes responsibility for the integrity of the data and the accuracy of the data analysis.

## DECLARATION OF INTERESTS

The authors declare no competing interests.

## INCLUSION AND DIVERSITY

We support inclusive, diverse, and equitable conduct of research.

Received: February 9, 2022
Revised: May 6, 2023
Accepted: July 11, 2023
Published: August 21, 2023

## REFERENCES

1. Funcke, J.B., and Scherer, P.E. (2019). Beyond adiponectin and leptin: adipose tissue-derived mediators of inter-organ communication. J. Lipid Res. *60*, 1648–1684. https://doi.org/10.1194/jlr.R094060.
2. Berg, A.H., Combs, T.P., and Scherer, P.E. (2002). ACRP30/adiponectin: an adipokine regulating glucose and lipid metabolism. Trends Endocrinol. Metab. *13*, 84–89.
3. Berg, A.H., Combs, T.P., Du, X., Brownlee, M., and Scherer, P.E. (2001). The adipocyte-secreted protein Acrp30 enhances hepatic insulin action. Nat. Med. *7*, 947–953. https://doi.org/10.1038/90992.
4. Straub, L.G., and Scherer, P.E. (2019). Metabolic Messengers: Adiponectin. Nat. Metab. *1*, 334–339. https://doi.org/10.1038/s42255-019-0041-z.
5. Liu, Y., Vu, V., and Sweeney, G. (2019). Examining the Potential of Developing and Implementing Use of Adiponectin-Targeted Therapeutics for Metabolic and Cardiovascular Diseases. Front. Endocrinol. *10*, 842. https://doi.org/10.3389/fendo.2019.00842.
6. Couch, Y., Buzàs, E.I., Di Vizio, D., Gho, Y.S., Harrison, P., Hill, A.F., Lötvall, J., Raposo, G., Stahl, P.D., Théry, C., et al. (2021). A brief history of nearly EV-erything - The rise and rise of extracellular vesicles. J. Extracell. Vesicles *10*, e12144. https://doi.org/10.1002/jev2.12144.
7. Le Lay, S., Rome, S., Loyer, X., and Nieto, L. (2021). Adipocyte-derived extracellular vesicles in health and diseases: Nano-packages with vast biological properties. FASEB Bioadv. *3*, 407–419. https://doi.org/10.1096/fba.2020-00147.
8. van Niel, G., D'Angelo, G., and Raposo, G. (2018). Shedding light on the cell biology of extracellular vesicles. Nat. Rev. Mol. Cell Biol. *19*, 213–228. https://doi.org/10.1038/nrm.2017.125.
9. Théry, C., Witwer, K.W., Aikawa, E., Alcaraz, M.J., Anderson, J.D., Andriantsitohaina, R., Antoniou, A., Arab, T., Archer, F., Atkin-Smith, G.K., et al. (2018). Minimal information for studies of extracellular vesicles 2018 (MISEV2018): a position statement of the International Society for Extracellular Vesicles and update of the MISEV2014 guidelines. J. Extracell. Vesicles *7*, 1535750. https://doi.org/10.1080/20013078.2018.1535750.
10. Stepanian, A., Bourguignat, L., Hennou, S., Coupaye, M., Hajage, D., Salomon, L., Alessi, M.C., Msika, S., and de Prost, D. (2013). Microparticle increase in severe obesity: Not related to metabolic syndrome and unchanged after massive weight loss. Obesity *21*, 2236–2243. https://doi.org/10.1002/oby.20365.
11. Amosse, J., Durcin, M., Malloci, M., Vergori, L., Fleury, A., Gagnadoux, F., Dubois, S., Simard, G., Boursier, J., Hue, O., et al. (2018). Phenotyping of circulating extracellular vesicles (EVs) in obesity identifies large EVs as functional conveyors of Macrophage Migration Inhibitory Factor. Mol. Metab. *18*, 134–142. https://doi.org/10.1016/j.molmet.2018.10.001.
12. Santamaria-Martos, F., Benitez, I.D., Latorre, J., Lluch, A., Moreno-Navarrete, J.M., Sabater, M., Ricart, W., Sanchez de la Torre, M., Mora, S.,

Fernández-Real, J.M., and Ortega, F.J. (2020). Comparative and functional analysis of plasma membrane-derived extracellular vesicles from obese vs. nonobese women. Clin. Nutr. *39*, 1067–1076. https://doi.org/10.1016/j.clnu.2019.04.008.

13. Li, S., Wei, J., Zhang, C., Li, X., Meng, W., Mo, X., Zhang, Q., Liu, Q., Ren, K., Du, R., et al. (2016). Cell-Derived Microparticles in Patients with Type 2 Diabetes Mellitus: a Systematic Review and Meta-Analysis. Cell. Physiol. Biochem. *39*, 2439–2450. https://doi.org/10.1159/000452512.
14. Freeman, D.W., Noren Hooten, N., Eitan, E., Green, J., Mode, N.A., Bodogai, M., Zhang, Y., Lehrmann, E., Zonderman, A.B., Biragyn, A., et al. (2018). Altered Extracellular Vesicle Concentration, Cargo and Function in Diabetes Mellitus. Diabetes. https://doi.org/10.2337/db17-1308.
15. Durcin, M., Fleury, A., Taillebois, E., Hilairet, G., Krupova, Z., Henry, C., Truchet, S., Trötzmüller, M., Köfeler, H., Mabilleau, G., et al. (2017). Characterisation of adipocyte-derived extracellular vesicle subtypes identifies distinct protein and lipid signatures for large and small extracellular vesicles. J. Extracell. Vesicles *6*, 1305677. https://doi.org/10.1080/20013078.2017.1305677.
16. Camino, T., Lago-Baameiro, N., Bravo, S.B., Sueiro, A., Couto, I., Santos, F., Baltar, J., Casanueva, F.F., and Pardo, M. (2020). Vesicles Shed by Pathological Murine Adipocytes Spread Pathology: Characterization and Functional Role of Insulin Resistant/Hypertrophied Adiposomes. Int. J. Mol. Sci. *21*, 2252. https://doi.org/10.3390/ijms21062252.
17. Mleczko, J., Ortega, F.J., Falcon-Perez, J.M., Wabitsch, M., Fernandez-Real, J.M., and Mora, S. (2018). Extracellular Vesicles from Hypoxic Adipocytes and Obese Subjects Reduce Insulin-Stimulated Glucose Uptake. Mol. Nutr. Food Res. *62*, 1700917. https://doi.org/10.1002/mnfr.201700917.
18. Deng, Z.B., Poliakov, A., Hardy, R.W., Clements, R., Liu, C., Liu, Y., Wang, J., Xiang, X., Zhang, S., Zhuang, X., et al. (2009). Adipose tissue exosome-like vesicles mediate activation of macrophage-induced insulin resistance. Diabetes *58*, 2498–2505. https://doi.org/10.2337/db09-0216.
19. Lazar, I., Clement, E., Dauvillier, S., Milhas, D., Ducoux-Petit, M., LeGonidec, S., Moro, C., Soldan, V., Dalle, S., Balor, S., et al. (2016). Adipocyte Exosomes Promote Melanoma Aggressiveness through Fatty Acid Oxidation: A Novel Mechanism Linking Obesity and Cancer. Cancer Res. *76*, 4051–4057. https://doi.org/10.1158/0008-5472.CAN-16-0651.
20. Ying, W., Riopel, M., Bandyopadhyay, G., Dong, Y., Birmingham, A., Seo, J.B., Ofrecio, J.M., Wollam, J., Hernandez-Carretero, A., Fu, W., et al. (2017). Adipose Tissue Macrophage-Derived Exosomal miRNAs Can Modulate In Vivo and In Vitro Insulin Sensitivity. Cell *171*, 372–384.e12. https://doi.org/10.1016/j.cell.2017.08.035.
21. Thomou, T., Mori, M.A., Dreyfuss, J.M., Konishi, M., Sakaguchi, M., Wolfrum, C., Rao, T.N., Winnay, J.N., Garcia-Martin, R., Grinspoon, S.K., et al. (2017). Adipose-derived circulating miRNAs regulate gene expression in other tissues. Nature *542*, 450–455. https://doi.org/10.1038/nature21365.
22. Kranendonk, M.E.G., Visseren, F.L.J., van Balkom, B.W.M., Nolte-'t Hoen, E.N.M., van Herwaarden, J.A., de Jager, W., Schipper, H.S., Brenkman, A.B., Verhaar, M.C., Wauben, M.H.M., and Kalkhoven, E. (2014). Human adipocyte extracellular vesicles in reciprocal signaling between adipocytes and macrophages. Obesity *22*, 1296–1308. https://doi.org/10.1002/oby.20679.
23. Crewe, C., Joffin, N., Rutkowski, J.M., Kim, M., Zhang, F., Towler, D.A., Gordillo, R., and Scherer, P.E. (2018). An Endothelial-to-Adipocyte Extracellular Vesicle Axis Governed by Metabolic State. Cell *175*, 695–708.e13. https://doi.org/10.1016/j.cell.2018.09.005.
24. Flaherty, S.E., 3rd, Grijalva, A., Xu, X., Ables, E., Nomani, A., and Ferrante, A.W., Jr. (2019). A lipase-independent pathway of lipid release and immune modulation by adipocytes. Science *363*, 989–993. https://doi.org/10.1126/science.aaw2586.
25. Crewe, C., Funcke, J.B., Li, S., Joffin, N., Gliniak, C.M., Ghaben, A.L., An, Y.A., Sadek, H.A., Gordillo, R., Akgul, Y., et al. (2021). Extracellular vesicle-based interorgan transport of mitochondria from energetically stressed adipocytes. Cell Metab. *33*, 1853–1868.e11. https://doi.org/10.1016/j.cmet.2021.08.002.
26. Buzas, E.I. (2022). Opportunities and challenges in studying the extracellular vesicle corona. Nat. Cell Biol. *24*, 1322–1325. https://doi.org/10.1038/s41556-022-00983-z.
27. Kang, M., Jordan, V., Blenkiron, C., and Chamley, L.W. (2021). Biodistribution of extracellular vesicles following administration into animals: A systematic review. J. Extracell. Vesicles *10*, e12085. https://doi.org/10.1002/jev2.12085.
28. Fantuzzi, G. (2013). Adiponectin in inflammatory and immune-mediated diseases. Cytokine *64*, 1–10. https://doi.org/10.1016/j.cyto.2013.06.317.
29. Pan, Y., Hui, X., Hoo, R.L.C., Ye, D., Chan, C.Y.C., Feng, T., Wang, Y., Lam, K.S.L., and Xu, A. (2019). Adipocyte-secreted exosomal microRNA-34a inhibits M2 macrophage polarization to promote obesity-induced adipose inflammation. J. Clin. Invest. *129*, 834–849. https://doi.org/10.1172/JCI123069.
30. Mathieu, M., Névo, N., Jouve, M., Valenzuela, J.I., Maurin, M., Verweij, F.J., Palmulli, R., Lankar, D., Dingli, F., Loew, D., et al. (2021). Specificities of exosome versus small ectosome secretion revealed by live intracellular tracking of CD63 and CD9. Nat. Commun. *12*, 4389. https://doi.org/10.1038/s41467-021-24384-2.
31. Mizunoe, Y., Kobayashi, M., Tagawa, R., Nakagawa, Y., Shimano, H., and Higami, Y. (2019). Association between Lysosomal Dysfunction and Obesity-Related Pathology: A Key Knowledge to Prevent Metabolic Syndrome. Int. J. Mol. Sci. *20*, 3688. https://doi.org/10.3390/ijms20153688.
32. Zhai, R., Pan, L., Yang, Z., Li, T., Ning, Z., Pawitan, Y., Wilson, J.F., Wu, D., and Shen, X. (2022). Genetic and phenotypic links between obesity and extracellular vesicles. Hum. Mol. Genet. *31*, 3643–3651. https://doi.org/10.1093/hmg/ddac069.
33. Camino, T., Lago-Baameiro, N., Bravo, S.B., Molares-Vila, A., Sueiro, A., Couto, I., Baltar, J., Casanueva, E.F., and Pardo, M. (2022). Human obese white adipose tissue sheds depot-specific extracellular vesicles and reveals candidate biomarkers for monitoring obesity and its comorbidities. Transl. Res. *239*, 85–102. https://doi.org/10.1016/j.trsl.2021.01.006.
34. Phoonsawat, W., Aoki-Yoshida, A., Tsuruta, T., and Sonoyama, K. (2014). Adiponectin is partially associated with exosomes in mouse serum. Biochem. Biophys. Res. Commun. *448*, 261–266. https://doi.org/10.1016/j.bbrc.2014.04.114.
35. Garcia-Martin, R., Brandao, B.B., Thomou, T., Altindis, E., and Kahn, C.R. (2022). Tissue differences in the exosomal/small extracellular vesicle proteome and their potential as indicators of altered tissue metabolism. Cell Rep. *38*, 110277. https://doi.org/10.1016/j.celrep.2021.110277.
36. Tóth, E.Á., Turiák, L., Visnovitz, T., Cserép, C., Mázló, A., Sódar, B.W., Försönits, A.I., Petővári, G., Sebestyén, A., Komlósi, Z., et al. (2021). Formation of a protein corona on the surface of extracellular vesicles in blood plasma. J. Extracell. Vesicles *10*, e12140. https://doi.org/10.1002/jev2.12140.
37. Yerneni, S.S., Solomon, T., Smith, J., and Campbell, P.G. (2022). Radioiodination of extravesicular surface constituents to study the biocorona, cell trafficking and storage stability of extracellular vesicles. Biochim. Biophys. Acta. Gen. Subj. *1866*, 130069. https://doi.org/10.1016/j.bbagen.2021.130069.
38. Obata, Y., Kita, S., Koyama, Y., Fukuda, S., Takeda, H., Takahashi, M., Fujishima, Y., Nagao, H., Masuda, S., Tanaka, Y., et al. (2018). Adiponectin/T-cadherin system enhances exosome biogenesis and decreases cellular ceramides by exosomal release. JCI Insight *3*, e99680. https://doi.org/10.1172/jci.insight.99680.
39. Kowal, J., Arras, G., Colombo, M., Jouve, M., Morath, J.P., Primdal-Bengtson, B., Dingli, F., Loew, D., Tkach, M., and Théry, C. (2016). Proteomic comparison defines novel markers to characterize heterogeneous populations of extracellular vesicle subtypes. Proc. Natl. Acad. Sci. USA *113*, E968–E977. https://doi.org/10.1073/pnas.1521230113.
40. Cnop, M., Havel, P.J., Utzschneider, K.M., Carr, D.B., Sinha, M.K., Boyko, E.J., Retzlaff, B.M., Knopp, R.H., Brunzell, J.D., and Kahn, S.E. (2003). Relationship of adiponectin to body fat distribution, insulin sensitivity and plasma lipoproteins: evidence for independent roles of age and sex. Diabetologia *46*, 459–469. https://doi.org/10.1007/s00125-003-1074-z.

41. Ying, W., Gao, H., Dos Reis, F.C.G., Bandyopadhyay, G., Ofrecio, J.M., Luo, Z., Ji, Y., Jin, Z., Ly, C., and Olefsky, J.M. (2021). MiR-690, an exosomal-derived miRNA from M2-polarized macrophages, improves insulin sensitivity in obese mice. Cell Metab. *33*, 781–790.e5. https://doi.org/10.1016/j.cmet.2020.12.019.

42. Kulaj, K., Harger, A., Bauer, M., Caliskan, Ö.S., Gupta, T.K., Chiang, D.M., Milbank, E., Reber, J., Karlas, A., Kotzbeck, P., et al. (2023). Adipocyte-derived extracellular vesicles increase insulin secretion through transport of insulinotropic protein cargo. Nat. Commun. *14*, 709. https://doi.org/10.1038/s41467-023-36148-1.

43. Xia, J.Y., Sun, K., Hepler, C., Ghaben, A.L., Gupta, R.K., An, Y.A., Holland, W.L., Morley, T.S., Adams, A.C., Gordillo, R., et al. (2018). Acute loss of adipose tissue-derived adiponectin triggers immediate metabolic deterioration in mice. Diabetologia *61*, 932–941. https://doi.org/10.1007/s00125-017-4516-8.

44. Wijesekara, N., Krishnamurthy, M., Bhattacharjee, A., Suhail, A., Sweeney, G., and Wheeler, M.B. (2010). Adiponectin-induced ERK and Akt phosphorylation protects against pancreatic beta cell apoptosis and increases insulin gene expression and secretion. J. Biol. Chem. *285*, 33623–33631. https://doi.org/10.1074/jbc.M109.085084.

45. Verweij, F.J., Revenu, C., Arras, G., Dingli, F., Loew, D., Pegtel, D.M., Follain, G., Allio, G., Goetz, J.G., Zimmermann, P., et al. (2019). Live Tracking of Inter-organ Communication by Endogenous Exosomes In Vivo. Dev. Cell *48*, 573–589.e4. https://doi.org/10.1016/j.devcel.2019.01.004.

46. Hyenne, V., Ghoroghi, S., Collot, M., Bons, J., Follain, G., Harlepp, S., Mary, B., Bauer, J., Mercier, L., Busnelli, I., et al. (2019). Studying the Fate of Tumor Extracellular Vesicles at High Spatiotemporal Resolution Using the Zebrafish Embryo. Dev. Cell *48*, 554–572.e7. https://doi.org/10.1016/j.devcel.2019.01.014.

47. Bing, C. (2015). Is interleukin-1beta a culprit in macrophage-adipocyte crosstalk in obesity? Adipocyte *4*, 149–152. https://doi.org/10.4161/21623945.2014.979661.

48. Hotamisligil, G.S., and Spiegelman, B.M. (1994). Tumor necrosis factor alpha: a key component of the obesity-diabetes link. Diabetes *43*, 1271–1278. https://doi.org/10.2337/diab.43.11.1271.

49. Ryu, J., Hadley, J.T., Li, Z., Dong, F., Xu, H., Xin, X., Zhang, Y., Chen, C., Li, S., Guo, X., et al. (2021). Adiponectin Alleviates Diet-Induced Inflammation in the Liver by Suppressing MCP-1 Expression and Macrophage Infiltration. Diabetes *70*, 1303–1316. https://doi.org/10.2337/db20-1073.

50. Ruan, H., and Dong, L.Q. (2016). Adiponectin signaling and function in insulin target tissues. J. Mol. Cell Biol. *8*, 101–109. https://doi.org/10.1093/jmcb/mjw014.

51. Claridge, B., Lozano, J., Poh, Q.H., and Greening, D.W. (2021). Development of Extracellular Vesicle Therapeutics: Challenges, Considerations, and Opportunities. Front. Cell Dev. Biol. *9*, 734720. https://doi.org/10.3389/fcell.2021.734720.

52. Pajvani, U.B., Du, X., Combs, T.P., Berg, A.H., Rajala, M.W., Schulthess, T., Engel, J., Brownlee, M., and Scherer, P.E. (2003). Structure-function studies of the adipocyte-secreted hormone Acrp30/adiponectin. Implications fpr metabolic regulation and bioactivity. J. Biol. Chem. *278*, 9073–9085. https://doi.org/10.1074/jbc.M207198200.

53. Bonsergent, E., Grisard, E., Buchrieser, J., Schwartz, O., Théry, C., and Lavieu, G. (2021). Quantitative characterization of extracellular vesicle uptake and content delivery within mammalian cells. Nat. Commun. *12*, 1864. https://doi.org/10.1038/s41467-021-22126-y.

54. O'Brien, K., Ughetto, S., Mahjoum, S., Nair, A.V., and Breakefield, X.O. (2022). Uptake, functionality, and re-release of extracellular vesicle-encapsulated cargo. Cell Rep. *39*, 110651. https://doi.org/10.1016/j.celrep.2022.110651.

55. Decaunes, P., Bouloumié, A., Ryden, M., and Galitzky, J. (2018). Ex vivo Analysis of Lipolysis in Human Subcutaneous Adipose Tissue Explants. Bio. Protoc. *8*, e2711.

56. Blandin, A., Dugail, I., Hilairet, G., Ponnaiah, M., Ghesquière, V., Froger, J., Ducheix, S., Fizanne, L., Boursier, J., Cariou, B., et al. (2023). Lipidomic analysis of adipose-derived extracellular vesicles reveals specific EV lipid sorting informative of the obesity metabolic state. Cell Rep. *42*, 112169. https://doi.org/10.1016/j.celrep.2023.112169.

57. Halberg, N., Schraw, T.D., Wang, Z.V., Kim, J.Y., Yi, J., Hamilton, M.P., Luby-Phelps, K., and Scherer, P.E. (2009). Systemic fate of the adipocyte-derived factor adiponectin. Diabetes *58*, 1961–1970. https://doi.org/10.2337/db08-1750.

58. Fleury, A., Hoch, L., Martinez, M.C., Faure, H., Taddei, M., Petricci, E., Manetti, F., Girard, N., Mann, A., Jacques, C., et al. (2016). Hedgehog associated to microparticles inhibits adipocyte differentiation via a non-canonical pathway. Sci. Rep. *6*, 23479. https://doi.org/10.1038/srep23479.

59. Briand, N., Prado, C., Mabilleau, G., Lasnier, F., Le Lièpvre, X., Covington, J.D., Ravussin, E., Le Lay, S., and Dugail, I. (2014). Caveolin-1 expression and cavin stability regulate caveolae dynamics in adipocyte lipid store fluctuation. Diabetes *63*, 4032–4044. https://doi.org/10.2337/db13-1961.

## STAR★METHODS

### KEY RESOURCES TABLE

| REAGENT or RESOURCE | SOURCE | IDENTIFIER |
|---|---|---|
| **Antibodies** | | |
| Adiponectin (murine) | Thermofisher Scientific | #PA1-054, RRID:AB_325789 |
| Adiponectin (human) | Abeomics | #10-7597, RRID:AB_2943077 |
| AKT pan (40D4) | Cell signaling | Cat #2920, RRID:AB_1147620 |
| AKT pan polyclonal (*in vivo* studies) | Cell signaling | Cat #4691, RRID:AB_915783 |
| Phospho-AKT (pAKT, Ser 473) | Cell signaling | Cat #4060S, RRID:AB_2315049 |
| Alix | BD Biosciences | Cat #611620, RRID:AB_399062 |
| Murine CD9 | BD Pharmingen | Cat #553758, RRID:AB_395032 |
| human CD9 | Santa Cruz | Cat #SC-13118, RRID:AB_627213 |
| Murine CD63 | MBL | Cat #D263-3, RRID:AB_1278815 |
| Flotillin-2 | BD Pharmingen | Cat #610383, RRID:AB_397766 |
| Mac2 | Cedarlane | Cat #CL8942AP, RRID:AB_10060357 |
| MIF (human) | R&D systems | Cat #mab289, RRID:AB_2281975 |
| Syntenin-1 | Abcam | Cat #ab19903, RRID:AB_445200 |
| Zs-Green | Clontech | Cat #632598, RRID:AB_2943078 |
| Goat anti-rat IgG2a Secondary antibody HRP conjugate (used for MaC2 staining) | Invitrogen | Cat# PA1-84709, RRID:AB_933942 |
| Anti-adiponectin FITC coupled antibody | Assay-Pro | Cat #10361-05041, RRID:AB_2943079 |
| IRDye® 800CW and 680RD secondary antibody (anti-mouse and anti-rabbit) | LI-COR Biosciences | Cat #926–32211, RRID:AB_621843; Cat #926–32210,RRID:AB_621842; Cat #926–68071, RRID:AB_10956166; Cat #926-68070, RRID:AB_10956588 |
| **Chemicals, peptides, and recombinant proteins** | | |
| Bovine serum albumin (BSA) FFA free | Sigma | Cat #A7030 |
| Collagenase A | Roche | Cat #10103586001 |
| DAB OB Super Sensitive detection kit | ImPath | Cat #46538 |
| DAB Quanto | Thermofischer Scientific | Cat #TA-125-QHDX |
| Wash buffer for IHC | ImPath | Cat #45002 |
| Antigen retrieval solution pH6.0 | ImPath | Cat #44998 |
| Ultravision Hydrogen Peroxyde block | Thermofisher Scientific | Cat #TS-12-H2O2Q |
| Goat serum | Immunoreagents | Cat #SP-004-VX10 |
| IHC mounting medium | CellPath | Cat #SEA-1604-00A |
| Qiazol Lysis reagent | Qiagen | Cat #79306 |
| RNeasy mini kit | Qiagen | Cat #74104 |
| SuperScriptII reverse Transcriptase | Invitrogen | Cat #18064-014 |
| dNTP set 100mM | Invitrogen | Cat #10297-018 |
| Random hexamers | Invitrogen | Cat #48190-011 |
| QIAquick PCR purification kit | Qiagen | Cat #28106 |
| RNaseOut Ribonuclease inhibitor | Invitrogen | Cat #10777-019 |
| Maxima SYBR Green qPCR master mix 2X | Thermofisher Scientific | Cat #K0253 |
| 96-Well PCR plates | Thermofisher Scientific | Cat #AB0700 |
| DMEM 4.5 g/L glucose | Gibco | Cat #41966-029 |
| DMEM 1 g/L glucose | Gibco | Cat #31885-023 |
| Elisa mouse Adiponectin/Acrp30 | R&DSystems | Cat #DY1119 and #DY008 |

(*Continued on next page*)

*Continued*

| REAGENT or RESOURCE | SOURCE | IDENTIFIER |
|---|---|---|
| Exosome isolation kit Pan, mouse | Miltenyi Biotec | Cat #120-041-065 |
| Fetal Calf serum (FCS) | Eurobio | Cat #CVFSVF00-01 |
| Insulin 100UI/mL | Lilly | Cat #HI0210 |
| Zeocin | Thermofisher Scientific | Cat #R25001 |
| Palmitate | Sigma | Cat #P-0500 |
| Proteinase K | Sigma Aldrich | Cat #P2308 |
| PMSF | Santa Cruz | Cat #SC24948 |
| ECBM | PromoCell | Cat #C22210 |
| Fetal Bovine serum | Gibco BRL | Cat #10270-106, Lot 42G2078K |
| Fluoromount-G | Invitrogen | Cat #00-4958-02 |
| Glutaraldehyde 25% solution | Electron microscopy Sciences | Cat #16220 |
| IRDye® 800CW NHS ester | LICOR | Cat #92970021 |
| Mini-Protean TGX gels | Bio-Rad | Cat #4568083, #4568086, |
| Mowiol | Calbiochem | Cat #475904 |
| Optiprep™ density gradient medium | Sigma Aldrich | Cat #D1556 |
| Odyssey blocking buffer (TBS) | LI-COR Biosciences | Cat #927-50010 |
| Paraformaldehyde 32% | Electron microscopy Sciences | Cat #15714 |
| Running buffer | Interchim | Cat #91495E |
| 4X Laemmli sample buffer | Bio-Rad | Cat #161-0747 |
| Triton X-100 | Sigma | Cat #T8787 |
| Trans-blot Turbo transfer reagents | Bio-Rad | Cat #10026938, #1704158, #1704271 |
| Trypsin 0.05% | Corning | Cat #25-051-CI |
| RNAiMax Lipofectamine | Invitrogen | Cat #12323563 |
| High-fat diet (HFD) 61% of the energy from fat (D12492 Premix AIN) | Safe diet | Cat# SAFE® 233 HF |
| **Critical commercial assays** | | |
| DC-protein assay | BioRad | Cat #5000111 |
| Mouse adipokine array kit | R&D systems | Cat #ARY013 |
| Mouse and human adiponectin/ Acrp30 DuoSet ELISA | R&D systems | Cat #DY1119 and DY1065 |
| Human magnetic Luminex set for adiponectin | Bio-Rad | Cat #171A7002M |
| Ultrasensitive mouse Elisa kit | Crystal Chem | Cat #90080 |
| Element RC liver rotor | Scil animal care company | Cat #AW00199 |
| Glucometer strips for glucometer AccuCheck Guide | Roche | Cat #08721106001 |
| Clinicells 25cm$^3$ | GEDTECH | Cat #00108 |
| **Experimental models: Cell lines** | | |
| HEK 293 | ATCC | Cat #CRL-1573 |
| HepG2 cells | ATCC | Cat #HB-8065 |
| Phoenix-AMPHO cells | ATCC | Cat #CRL-3213 |
| Experimental models: Organisms/strains | | |
| Ob/Ob mice | Charles River | B6.Cg-Lep$^{ob}$/J, stock N° 000632, JAX™ mice strain |
| RCL-ZsGreen | The Jackson Laboratory | B6.Cg-Gt(ROSA)26Sor$^{tm6(CAG-ZsGreen1)Hze}$/J, stock N°007906, JAX™ mice strain |

(*Continued on next page*)

| Continued | | |
|---|---|---|
| REAGENT or RESOURCE | SOURCE | IDENTIFIER |
| Adipoq- Cre-ERT2 | The Jackson Laboratory | C57BL/6-Tg(Adipoq-cre/ERT2)1Soff/J, stock N°025124, JAX™ mice strain |
| Adiponectin KO mice (Adpn KO) | The Jackson Laboratory | B6; 129-Adipoq$^{tm1Chan}$/J, stock N° 008195 |
| Oligonucleotides | | |
| ON-TARGETplus Non-targeting pool, 5 nmol | Horizon Discoveries | Cat #J-007800-10-0005 |
| ON-TARGETplus human ADIPOR1 (51094) siRNA individual, 5 nmol | Horizon Discoveries | Cat #J-007800-10-0005 |
| ON-TARGETplus human ADIPOR2 (79602) siRNA individual, 5 nmol | Horizon Discoveries | Cat # D-001810-10-05 |
| Recombinant DNA | | |
| Venus-adiponectin lentiviral plasmid | Kind gift from Weiping Han | Laboratory of metabolic Medicine, Singapore Bioimaging Consortium |
| Software and algorithms | | |
| Image Studio software | LI-COR Biosciences | Biosciences https://www.licor.com/bio/products/software/image_studio/ |
| ImageJ | Downloaded from https://imagej.nih.gov/ij/ | https://imagej.nih.gov/ij/ |
| Nanosight NTA software (version 3.1) | Malvern Panalytical | https://www.malvernpanalytical.com/en/support/product-support/software/NanoSight-NTA-software-update-v3-10-l2 |
| Bioplex manager software (version 4.1.1) | Bio Rad | http://www.bio-rad.com/fr-fr/product/bio-plex-manager-software-standard-edition?ID=5846e84e-03a7-4599-a8ae-7ba5dd2c7684 |
| GraphPad Prism | GraphPad | https://www.graphpad.com/scientific-software/prism/ |

## RESOURCE AVAILABILITY

### Lead contact

Further information and requests for resources and reagents should be directed to and will be fulfilled by the lead contact, Soazig le Lay (soazig.lelay@inserm.fr).

### Materials availability

This study did not generate new unique reagents.

All key resources and product references used in this study are presented as supplemental material in a key resource table (KRT).

### Data and code availability

- Data are available on request by email to soazig.lelay@inserm.fr.
- This paper do not contain original code.
- Any additional information required to reanalyze the data reported in this paper is available from the Lead contact upon request.

## EXPERIMENTAL MODEL AND SUBJECT DETAILS

### Human studies

The institutional ethics committee approved the study, and consent was obtained from each patient. Patients with metabolic syndrome (MS) were included from the NUMEVOX cohort (NCT00997165) at the Department of Endocrinology and Nutrition of Angers University Hospital according to eligibility criteria previously described.[11] Twenty-seven patients with MS (11 females/16 males) were stratified into two groups according to their BMI (in kg.m$^{-2}$), namely, 10 overweight patients (27<BMI<30) and 17 obese patients (BMI>30), and were compared to 8 control patients (4 females/4 males, BMI <27). Clinical parameters of the patients included in the study were measured as previously described[11] and are presented in Table S1. A BMI of 27 kg/m$^2$ was used to distinguish between lean and moderately overweight subjects to mirror the cut off retained for pharmacotherapy adjunction in patients with

concomitant obesity-related risk factors, as is the case for people with metabolic syndrome. Plasma adiponectin levels were also measured in a limited number of samples (control, n = 3 (1 female/2 males); overweight, n = 5 (1 female/4 males); obese, n = 5 (4 females/1 male)) and were further correlated with plasma adiponectin$^{+}$ EVs detected by flow cytometry in the same patients.

Human adipose tissue explants were collected from three fat depots (mesenteric, omental and subcutaneous) from patients undergoing bariatric surgery and were included in the prospective monocentric METABOSE cohort (Nutrition Department, CHU Tours) following patient written consent and after local ethics committee agreement (CNIL no. 18254562). The clinical parameters of the patients included in the study are presented in Table S2.

### Animal experimentation and *in vivo* EV treatment

Adult mice heterozygous (*ob*/+) for the leptin spontaneous mutation Lep$^{ob}$ were initially obtained from Charles River (B6.Cg-*Lep* $^{ob}$/J, Stock No. 000632, JAX mice strain) and were interbred to obtain a colony. Regular backcross with commercial Lep$^{ob/+}$ was performed to avoid any background drift. Three-to five-month-old lean (*ob*/+ or +/+) or obese (*ob*/*ob*) mice were used for plasma collection following intracardiac puncture and adipose tissue dissection.

Mice specifically expressing Zs-Green in adipocytes (AdipoZS1) were obtained following the crossing of RCL-ZsGreen (B6.Cg-Gt(ROSA)26Sor$^{tm6(CAG-ZsGreen1)Hze/J}$, Stock No. 007906, JAX mice strain) with mice expressing a tamoxifen-inducible cre recombinase, Cre-ERT2, under the control of the adiponectin gene promoter (C57BL/6-Tg(Adipoq-cre/ERT2)1Soff/J, Stock No. 025124, JAX mice strain).

Adipocyte-specific Adiponectin KO (Adpn-KO) mice were obtained from the Jackson Laboratory (B6; 129-Adipoq$^{tm1Chan}$/J, Stock No. 008195) and were interbred to obtain a colony.

Male C57BL/6 (B6) mice were fed a high-fat diet (HFD) (61% of calories from fat, 20% of calories from protein, and 20% of calories from carbohydrate, #D12492, Safe Diets) or a normal chow diet *ad libitum* directly after weaning (at 4–5 weeks of age) for a period of 5 weeks. During this HFD feeding period, visceral adipose tissue (VAT)-derived EVs were adoptively transferred into recipient mice twice a week by intraperitoneal injection (i.p.). Each injection contained 5 μg of EV proteins resuspended in 100 μL of 0.9% NaCl, a quantity that was chosen since it corresponds to the EV protein mean quantity secreted by 500 mg of VAT (which corresponds to the mean VAT weight of lean mice) over 48 h. In the control groups, 100 μL of sterile 0.9% NaCl was injected as the vehicle.

All mice had *ad libitum* access to food and water and were housed in the same open mouse facility on a 12/12-h light/dark day/night cycle. Animal care and study protocols were approved by the French Ministry of Education and Research and the ethics committee N°6 in animal experimentation and were in accordance with the EU Directive 2010/63/EU for animal experiments. At sacrifice, mouse tissues were collected and used as explants for EV production or were fixed in 10% formalin for immunohistochemistry or frozen in liquid nitrogen and stored at −80°C for protein lysates.

## METHOD DETAILS

### Measurement of serum liver metabolic parameters

We used the chemistry analyzer Element RC (Scil Animal Care Company) with Element RC liver rotors to determine the concentrations of total proteins, albumin, total cholesterol, and bilirubin and aminotransferase (alanine aminotransferase [ALT], aspartate aminotransferase [AST] and alkaline aminotransferase [ALP]) activities in mouse serum. The reagent rotor sample chamber was loaded with 50–100 μL of serum according to available samples and the rotor inserted. Sample values were compared with standardized mouse ranges, with internal quality control (QC) monitors on the analyzer, rotor, and sample before and during analysis to ensure reliable, consistent results. Each of the individual rotors used for analysis passed all QC parameters as indicated when the test was complete.

### Metabolic tolerance test

The glucose tolerance test (GTT) and insulin tolerance test (ITT) were performed in the 4$^{th}$ week of sEV injections. Food was removed 6 h before the initiation of the tolerance tests. For the GTT, a single dose of glucose (2 g/kg) was administered by intraperitoneal (i.p.) injection at time 0. For ITT, mice were injected i.p. with 0.5 IU/kg body weight insulin at time 0. Blood glucose levels were monitored using glucometer strips at 0, 15, 30, 45, 60, 90 and 120 min on 2.5-μL samples collected from the tail. GTT and ITT were also performed on standard diet (SD)-fed mice as a control for normal glucose and insulin tolerance responses.

### Insulin-stimulated AKT phosphorylation assay

EV-associated adiponectin insulin-sensitizing effects were evaluated by measuring insulin-stimulated AKT phosphorylation on serine 473 in insulin cells/target tissues.

For *in vitro* experiments, palmitate-treated hepatocytes incubated or not with sEVs (as described in the cell culture section) were treated for 5 min with insulin (100 nM) prior to protein lysate preparation. One representative blot together with the quantification of the *p*-Akt/Akt ratio as a fold increase over basal conditions (NaCl) are presented.

For *in vivo* experiments, the phosphorylation of AKT in response to 0.5 U/kg body weight insulin injection in the *vena cava* of 6-h-fasted mice was studied in tissue lysates collected at different time points following insulin stimulation: liver at 3 min, skeletal muscle at 7 min and VAT at 10 min. One animal of each group (NaCl, Lean sEVs, and AdpnKO sEVs) was sequentially sacrificed. Paired

animal trios were further analyzed with the pAKT/AKT ratio for NaCl conditions (within each trio) set to 1 and the pAKT/AKT ratio for sEV-treated animals expressed as the fold increase over NaCl.

### Primary adipocytes and adipose tissue explant culture

Three to four grams of mouse AT was used for collagenase adipocyte isolation as previously described[15] or minced into small pieces for VAT, subcutaneous AT (SAT) or brown adipose tissue (BAT) explants. Adipocyte or AT explant cultures were placed into a Clinicell 25 cassette filled with 10 mL of ECBM/HEPES 10 mM/0.1% FFA-free BSA pH 7.4 as previously described.[55] Serum-free conditioned medium (CM) after 48 h of culture was collected, filtered through a 100-μm cell strainer and used for EV isolation.

### AT-derived EV isolation

CM was first spun at 1,500x*g* for 20 min to remove cells and cell debris. lEVs were recovered from cell-cleared supernatants (1,500x*g* for 20 min) by centrifugation for 60 min at 13,000*xg*, followed by two washing steps in NaCl and resuspension in sterile 0.9% NaCl. sEVs were further isolated from lEV-depleted supernatants following a 100,000x*g* ultracentrifugation step for 1 h at 4°C (rotor MLA-50, Beckman Coulter Optima MAX-XP Ultracentrifuge) and two washes in NaCl. The EV protein content was estimated by a DC-protein assay kit by using BSA as a standard. The purity of isolated EVs was checked on density gradients by loading 20–45 μg of each EV subtype at the bottom of an iodixanol density gradient as previously described[39] with adaptations to fit the gradient in tubes required for the MLS-50 rotor. Briefly, EVs were resuspended in 1.35 mL of buffer containing 0.25 M sucrose, 10 mM Tris (pH 8.0), and 1 mM EDTA (pH 7.4) and mixed 1:1 with a 60% (w/v) stock solution of iodixanol/Optiprep. Next, 1.2 mL and 1.1 mL of 20% and 10% iodixanol solutions were successively layered on top of the vesicles, and the tubes were centrifuged for 2.5 h at 268,000x*g* at 4°C in MLS-50. Ten fractions of 500 μL were collected from the top of the tube. Density fractions were assessed with a refractometer (R-5000, Atago). Fractions collected were then diluted with 500 μL of PBS and ultracentrifuged for 30 min at 100,000*xg* in an MLA-130 rotor. Concentrated fractions were resuspended in 22.5 μL of PBS and loaded on Western blot gels. AT-derived EVs were measured by NTA and expressed per gram of source AT. Since AT cellularity between lean and obese mice differs because of obesity-associated adipocyte hypertrophy, we normalized the expression of adipose EV secretion by total mouse AT (calculated by multiplying the EVs secreted per gram of AT by the mean AT weight of lean or obese mice, respectively) when the two phenotypes were compared.

### Plasma/serum EV isolation

Mouse and human peripheral blood were collected in EDTA-coated tubes as previously described.[11] Platelet-free plasma (PFP) was subjected to two series of centrifugations, each at 21,000x*g* for 45 min to pellet lEVs. The lEV-depleted PFP was further ultracentrifuged two times at 100,000x*g* for 1 h to isolate sEVs. PFP adiponectin concentrations were measured using 2 μL of PFP and total EV-depleted PFP samples according to the adiponectin ELISA kit manufacturer's protocol (R&D systems). Mouse serum was collected in heparinized capillary tubes, and EV-free serum was prepared following the ultracentrifugation protocol described for EV-depleted PFP.

### ELISA adiponectin measurement

The adiponectin concentration was measured using commercial ELISA kits (R&D systems) designed to measure full-length human or mouse adiponectin (Adpn) levels according to the manufacturer's protocol. One hundred microliters of diluted PFP or EV samples (final dilution 1/1000 to 1/10,000 for PFP samples and 1/50 to 1/500 for EV samples using the 1X diluent reagent provided in the kit) was used. The capture and HRP-conjugated detection antibodies as well as the calibrator provided in the total adiponectin ELISA kit were used. After substrate solution incubation, the optical density at 450 nm was read with a CLARIOstar Plus plate reader and corrected by the optical density read at 570 nm. Adpn concentrations were calculated from a four-parameter logistic (4-PL) standard curve fitting. EV samples prepared for a concurrent study using 3-month HFD-fed mice have been used to determine the Adpn content of HFD or SD VAT-derived sEVs.[56]

### Adiponectin clearance

The clearance of native adiponectin was determined by injecting 200 μL of wild-type serum or EV-free serum (following serum-EV depletion by two 100,000x*g* ultracentrifugations for 1 h each), both diluted to one-quarter in NaCl, into the tail vein of 8-week-old Adpn-KO mice as previously described.[57] Blood samples were subsequently collected at the indicated time points in heparinized capillary tubes. The levels of circulating adiponectin at various time points in Adpn-KO mice were determined by adiponectin measurement using a commercial ELISA kit following the manufacturer's protocol (R&D Systems).

### Mouse EV biodistribution

A total of 66 μg of AT-derived sEV protein was labeled with 800CW N-hydroxysuccinimide (NHS)-ester IRDye at a ratio of 0.03 mg dye to 1 mg EV total protein in a final volume of 100 μL of sterile 0.9% NaCl according to the manufacturer's instructions (LICOR Biosciences). Labeled EVs were recentrifuged (100,000x*g* for 1 h), and the EV pellet was resuspended in 100 μL of 0.9% sterile NaCl. The total volume of labeled EVs was injected via i.p. or intravenous (tail vein) injections in lean B6 control mice. Organ fluorescent background was also evaluated following the injection of 100 μL of 0.9% NaCl or EV-free NHS-ester labeling supernatant.

Mice were sacrificed 3 h post-injection, and organs were collected immediately and then imaged with a Licor Odyssey infrared imager to evaluate the labeled sEV biodistribution. Each organ was demarcated, and then the fluorescence intensity was measured in the respective organ surface with ImageJ software and expressed as the fluorescence intensity per surface unit.

### EV enzymatic assays

Twenty micrograms of EVs were incubated with 20 μg/mL proteinase K (PK) in the presence or absence of 1% Triton X-100 or left untreated in a final volume of 1 mL for 1 h at 37°C. PMSF (5 mM) was added for 5 min at 37°C, and PK was inactivated by placing the assay mixture at 90°C for 10 min. Similarly, EVs were either incubated with 0.25% trypsin-EDTA or left untreated in a final volume of 200 μL for 20 min at 37°C. EV-free serum was added to inactivate trypsin. Trypsin-treated EVs were further enriched by adiponectin following incubation with 500 μL of EV-depleted VAT conditioned medium. Following enzymatic treatment, lEVs and sEVs were re-pelleted at 13,000x*g* or 100,000x*g* for 1 h, resuspended in 22.5 μL of PBS and loaded on Western blot gels.

### Cell culture

HepG2 cells were maintained in high-glucose DMEM with 10% FBS at 37°C and seeded in 6-well plates (200,000 cells/well) for experiments. Before the experiments, the culture medium was changed to low-glucose DMEM with 0.5% BSA for 5 h, and then 0.3 mM palmitate was added for 24 h to induce insulin resistance. Hepatocytes, either rendered insulin resistant following palmitate exposure or not, were incubated for 24 h with different sEV concentrations (5, 10 or 20 μg/mL) as indicated in Figure 3A. The concentration of 10 μg/mL sEVs was classically used as a reference in other figures, as we previously demonstrated the sEV-induced cellular effects at this concentration without inducing any detrimental cellular effects.[58] Insulin response was evaluated by measuring Akt phosphorylation in cell lysates following 100 nM insulin stimulation for 5 min. Transfection of predesigned siRNA was performed in high-glucose DMEM supplemented with 10% FBS using 25 nM siRNA and RNAiMax Lipofectamine according to the manufacturer's instructions (Invitrogen).

Fluorescent Venus-tagged adiponectin (Adpn-Venus) or Venus tag (Venus) lentiviral plasmids were transfected into packaging cells to produce lentiviral particles used to further infect HEK293 cells as previously described.[59] Stable Adpn-Venus- or Venus-expressing HEK293 cells were selected and maintained by Zeocin selection (250 μg/mL) in high-glucose DMEM with 10% FBS. Stable Adpn-Venus HEK293 cells, displaying high Adpn or Venus expression, were then cultured in 15-cm cell culture plates in high-glucose DMEM with 10% FBS. The medium was then changed to serum-deprived media for 48 h to allow collection of HEK293 conditioned media from which Adpn-Venus or Venus sEVs were isolated following the classical 100,000x*g* ultracentrifugation procedure. For internalization experiments, HepG2 cells were seeded on glass coverslips, incubated with 10 μg/mL Adpn-Venus sEVs, fixed with 4% PFA and mounted in Mowiol at the different time points presented. After DAPI staining, sEV internalization was visualized by confocal laser fluorescence (Zeiss LSM 710). Fluorescence quantification was performed using ImageJ software. Quantification of Adpn-sEV Venus internalization is presented as the percentage of cell fluorescence, with the 24-h time point set to 100%.

### Western blot

Protein lysates (5–10 μg) were prepared and subjected to SDS–PAGE for western blotting as previously described.[15] Detection of adiponectin multimeric forms was achieved through the migration of samples under nonreducing conditions (DTT was excluded from the Laemmli buffer) and unheated conditions. IRDye (LI-COR Biosciences) secondary antibodies were used, and digital fluorescence was visualized by an Odyssey CLX system (LICOR). Immunoblot quantification was performed following analysis of the protein signal by Image Studio software. The antibodies used are listed in the KRT Table, and one representative blot for each protein is presented (among the mentioned independent experiments performed).

### Reverse transcription (RT)–quantitative PCR (qPCR)

RNA was isolated from tissues frozen in liquid nitrogen by homogenization in TRIzol Reagent, and RNA extraction was performed using an RNeasy RNA extraction kit (Qiagen) according to the manufacturer's protocol. RNA yield and quality were determined using a NanoDrop 2000 instrument (Thermo Fisher Scientific). One microgram of RNA was used to transcribe cDNA using a SuperScript II kit (Invitrogen). Quantitative PCR was performed using SYBR Green reagent with the LightCycler 480 apparatus (Roche) using validated qPCR primers (primer sequences are available upon request). The messenger RNA levels were calculated using the comparative threshold cycle (ΔΔCt) method by using 36B4 mRNA as a reference gene to normalize mRNA levels.

### Nanoparticle tracking analysis (NTA)

The EV concentration and size were determined by NTA (NanoSight NS300 equipped with a 405-nm laser, Malvern Instruments), as previously described.[15] EV samples were diluted 100-fold in sterile 0.9% NaCl prior to NTA. Video imaging was recorded with optimized set parameters (the detection threshold was set to 7 and 5 for lEVs and sEVs, respectively). Temperature was automatically monitored and ranged from 20°C to 21°C. Videos were analyzed when a sufficient number of valid trajectories were measured. Data capture and further analysis were performed using NTA software version 3.1. At least three independent biological samples of each EV subtype were analyzed, and the presented results correspond to the mean of the five videos taken for a given biological sample. Since NTA has reduced sensitivity for EVs smaller than ~70 nm, this would likely result in an overestimation of EV sizes and an underestimation of the differences between the lEV and sEV population sizes.

### sEV immunocapture

An alternative immunocapture-based method was also used to confirm the presence of adiponectin in VAT-derived EVs by using the exosome isolation kit pan CD9/CD63/CD81 according to the manufacturer's protocol (Miltenyi Biotec). Briefly, 50 μL of exosome isolation microbeads were incubated for 1 h with 2 mL of precleared VAT explant supernatants prior to loading on an equilibrated "μ" column placed in the magnetic field of the quadroMACS separator (Miltenyi Biotec). After four washes with isolation buffer, elution of $CD9^+CD63^+CD81^+$ sEVs was performed by placing the column outside of the magnetic separator, and the labeled vesicles were flushed out. Eluted sEVs were further used for Western blot analysis.

### Protein arrays

Mouse adipokine array kits were incubated with 50 μg of each EV subtype (lEVs or sEVs), isolated from either 48-h conditioned media from VAT explants or VAT-digested collagenase isolated adipocytes, and processed according to the manufacturer's protocol (R&D systems). Protein signals were revealed using a ChemiSmart 500 imager (Vilber Lourmat). The signal intensity of spots (two per protein, measured as the pixel number) was quantified using ImageJ software and expressed as the pixel mean of the two spots/μg of protein loaded on the membrane. The results presented are the mean signal intensity (mean pixels per μg of protein) obtained for each protein out of two independent blotting experiments. Only detectable protein signals out of the 38 adipokines tested are presented (see the list in Figure S1C).

### Flow cytometry assays

Flow cytometry lEV phenotyping was performed for the analysis of PFP as previously described.[11] Five microliters of PFP was fixed with 2% PFA in PBS for 15 min at room temperature and then washed with 1.5 mL of PBS and used for adiponectin detection. lEVs were pelleted (21,000x*g*, 15 min) and permeabilized with 100 μL of PBS/0.1% saponin for 5 min at RT prior to incubation with 10 μL of FITC-conjugated specific antibody. Irrelevant human immunoglobulin G (IgG) was used as an isotype-matched negative control for each sample and subtracted from the value obtained. The data obtained are expressed as a percentage of the total EVs analyzed.

### Histology and immunostaining

VAT, liver and muscles were excised and fixed in 10% PBS-buffered formalin for at least 24 h. Tissues were paraffin-embedded and sectioned (5 μm). Tissue sections were deparaffinized and rehydrated with specific commercial solutions (Impath). Following hydration, the tissues were stained with hematoxylin and eosin (HE) to assess the structural morphology. The diameter of the adipocytes was automatically calculated by a plugin specifically developed for HE images in ImageJ software.

For immunostaining, tissue sections were sequentially incubated in antigen retrieval solution (20 min, 101°C), hydroxide peroxide blocking solution (10 min), and washing solution (5 min) and blocked with goat serum (1.5%, 30 min) prior to incubation with Mac2 antibody (1/1000, 1 h). After washing, tissue sections were incubated with HRP-conjugated antibody (1/200, 30 min) prior to visualization with DAB (3,3′-diaminobenzidine). Counterstaining was carried out with hematoxylin prior to mounting. Isotype controls were routinely included.

## QUANTIFICATION AND STATISTICAL ANALYSIS

Data were analyzed using GraphPad Prism Software and are presented as dot plots representing independent experiments. Statistical analysis of the results was performed by using adapted statistical tests indicated in the figure legends. The differences were considered significant when the p value $\leq 0.05$ and are stated as follows: *$p \leq 0.05$, **$p \leq 0.01$, ***$p \leq 0.005$ and ****$p \leq 0.001$.